Article

Enzymatic Preparation of 2‘-5‘, 3‘-5‘Cyclic Dinucleotides, Their Binding Properties to STING Adaptor Protein, and Structure/Activity Correlations

Barbora Novotná, Lenka Vaneková, Martin Zav#el, Miloš Bud#šínský, Milan Dejmek, Miroslav Smola, Ondrej Gutten, Zahra Aliakbar Tehrani, Markéta Pimková Polidarová, Andrea Brázdová, Radek Liboska, Ivan Št#pánek, Zdenek Vavrina, Tomáš Jandušík, Radim Nencka, Lubomír Rulíšek, Evžen Bou#a, Ji#í Brynda, Ond#ej Páv, and Gabriel Birkus

J. Med. Chem., **Just Accepted Manuscript** • DOI: 10.1021/acs.jmedchem.9b01062 • Publication Date (Web): 12 Nov 2019

Enzymatic Preparation of 2‘-5‘, 3‘-5‘Cyclic Dinucleotides, Their Binding Properties to STING Adaptor Protein, and Structure/Activity Correlations

*Barbora Novotná[1,2], Lenka Vaneková[1,2], Martin Zavřel[1], Miloš Buděšínský[1], Milan Dejmek[1], Miroslav Smola[1], Ondrej Gutten[1], Zahra Aliakbar Tehrani[1], Markéta Pimková Polidarová[1,2], Andrea Brázdová[1], Radek Liboska[1], Ivan Štěpánek[1], Zdeněk Vavřina[1,2], Tomáš Jandušík[1,3], Radim Nencka[1], Lubomír Rulíšek[1], Evžen Bouřa[1], Jiří Brynda[1], Ondřej Páv[1] and Gabriel Birkuš[1,]**

[1] Institute of Organic Chemistry and Biochemistry of the Czech Academy of Sciences and Gilead Sciences Research Centre at IOCB, Flemingovo nam. 2, Prague, 16610, Czech Republic

[2] Faculty of Science, Charles University, Prague, Czech Republic

[3] Faculty of Food and Biochemical Technology, University of Chemistry and Technology, Prague, Czech Republic

ABSTRACT

Cyclic dinucleotides are second messengers in the cGAS-STING pathway which plays an important role in recognizing tumor cells and viral or bacterial infections. They bind to the STING adaptor protein and trigger expression of cytokines via TBK1/IRF3 and IKK/NFκB signaling cascades. In this report we describe an enzymatic preparation of 2'-5', 3'-5' cyclic dinucleotides (2'3'CDNs) with use of cyclic GMP-AMP synthases (cGAS) from human, mouse and chicken. We profile substrate specificity of these enzymes by employing a small library of NTP analogues and use them to prepare thirty-three 2'3'CDNs. We also determine affinity of these CDNs to five different STING haplotypes in cell-based and biochemical assays, and describe properties needed for their optimal activity toward all STING haplotypes. Next, we study their effect on cytokines and chemokines induction by human peripheral blood mononuclear cells (PBMC) and evaluate their cytotoxic effect on monocytes. Additionally, we report X-ray crystal structures of two new CDNs bound to STING protein and discuss structure activity relationship by using quantum and molecular mechanical (QM/MM) computational modeling.

INTRODUCTION

Cyclic dinucleotides (CDNs) play an important role as second messengers in vertebrates and prokaryotes.[1–3] They are naturally synthesized from NTPs by cyclic dinucleotide synthases. Prokaryotic and vertebrate CDNs differ in the type of phosphodiester linkages connecting two nucleotide monophosphates together. While bacteria produce 3'3'CDNs (e.g. 3'3'c-diGMP, 3'3'c-diAMP, 3'3'cGAMP) with two 3'-5' phosphodiester bonds,[4–6] only one CDN with mixed 2'-5' and 3'-5' phosphodiester linkage (2'3'cGAMP) is found in mammalian cells.[7]

2'3'cGAMP is a product of cyclic-GMP-AMP (cGAMP) synthase which is evolutionary conserved from fish to human.[2,8,9] The enzyme belongs to a family of DNA sensors and detects dsDNA released into cytosol during pathogen infection or disruption of host homeostasis.[10] Binding of dsDNA to cGAS occurs in a sequence-independent manner and induces a conformational change ultimately allowing synthesis of 2'3'cGAMP from ATP and GTP.[11] The 2'3' and 3'3' CDNs bind to an adaptor protein called Stimulator of Interferon Genes (STING, also denoted as TMEM173, MITA, ERIS) residing in endoplasmic reticulum.[12] STING is a 379 amino acid long protein consisting of the N-terminal transmembrane domain, the C-terminal ligand-binding domain and C-terminal tail (CTT).[11,13] Upon a CDN binding, STING homodimer transforms from an open to closed conformation and forms oligomers.[8] This conformation change leads to the recruitment of TBK1 kinase, trans-phosphorylation of CTT of STING and subsequent recruitment and phosphorylation of the transcription factor IRF3.[14–17] IRF3 then forms homodimers that translocate to the nucleus where they trigger expression of type I and III interferons. In parallel, a crosstalk between TBK1 and IKKβ kinases leads to NFκB activation and TNFα and IL-6 expression.[18]

cGAS-STING pathway plays an essential role in host defense against invading pathogens and in immune surveillance of tumor cells.[12,19] Its importance from the perspective of drug discovery is

highlighted by the fact that two cyclic dinucleotides ADU-S100 and MK-1454 are currently undergoing evaluation in Phase I clinical trials for the treatment of cancer.[20,21] Moreover CDNs could also find utility in the treatment of viral infections such as chronic hepatitis B, human immunodeficiency virus (HIV) infection or as adjuvants in vaccines.[22,23]

Several synthetic routes for 2'3' and 3'3' CDN preparations have been established.[24–26] However, these are usually complex multistep syntheses. Meanwhile, an elegant idea of using dinucleotide synthases for CDN preparation was pursued and few 3'3' and 2'3'CDNs were thus enzymatically prepared from the commercially available ATP and GTP analogues.[7,27–30]

The objective of this study is to identify the most suitable enzyme for synthesis of 2'3' CDNs, characterize binding properties of prepared CDNs toward STING adaptor protein and determine structure activity relations between STING and CDNs. To achieve this goal, we profile substrate specificity of chicken, mouse and human cGAS using a library of forty-one NTP analogues and describe preparation of thirty-three 2'3'CDNs. We characterize affinity of prepared CDNs toward five STING haplotypes in cell-based and biochemical assays. We also study their effect on induction of cytokines and chemokines by employing human peripheral blood mononuclear cells (PBMC) and evaluate their cytotoxic effect specifically on monocytes. Finally, we also discuss a structure–activity relationship (SAR) between prepared molecules and their biological activity by employing state-of-the-art methods of computational chemistry, such as QM/MM calculations.

RESULTS

Substrate specificity of human, mouse and chicken cGAS

Binding of DNA to cGAS triggers rearrangement of its active site and catalysis of 2'-5' phosphodiester bond between 2'-OH of GTP and α-phosphate of ATP.[11,29] The formed intermediate AMP-2'-GTP flips in the active site of the enzyme and 3'-5' phosphodiester bond between 3'-OH group of AMP and α-phosphate of GTP is formed.[11,29] Despite being responsible for the synthesis of the same product, cGAS from different species have relatively low amino acid homology. For example, human and mouse or human and chicken cGAS share 56% and 51% amino acid identity, respectively, based on BLAST® alignment[31] of amino acid sequences Q8C6L5, Q8N884 (UNIPROT) and XP_419881.4 (NCBI). Because of low level homology of cGAS from these three species, we decided to express them and profile their substrate specificity with a goal to identify the most suitable enzyme for synthesis of CDNs. We performed a small-scale synthesis of CDNs in such a way that one of the NTPs was always either ATP or GTP and the other an NTP analogue **1-41** (Tables 1A-1B).

For the arbitrarily chosen cut-off of >25% reaction conversion, twenty-eight CDNs could be prepared using mouse cGAS (mcGAS) compared to sixteen and eleven CDNs that could be made with human (hcGAS) and chicken (ccGAS) cGAS, respectively (Tables 1A-1B). Thus, mouse cGAS shows the lowest substrate specificity and is the most suited for enzymatic synthesis of CDNs. Nevertheless, human and chicken cGAS should not be disregarded. For example, human cGAS more efficiently catalyzed the reaction of GTP with 2-aminoadenosine-5'-triphosphate (**3)** or isoguanosine-5'-triphosphate (**4**), and the conversion of ATP with O^6-methylguanosine-5'-triphosphate (**16)** to the appropriate CDN was only possible with human cGAS (Table 1A).

Table 1A. Substrate specificity of human, mouse and chicken cGAS toward NTP analogues.

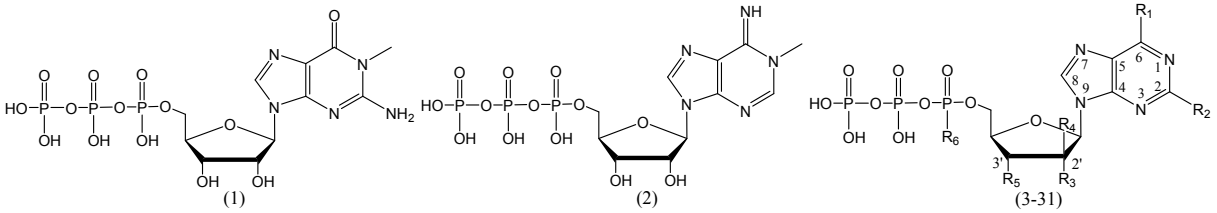

							Reaction Conversion (%)[a]					
							GTP			ATP		
NTP	R_1	R_2	R_3	R_4	R_5	R_6	hcGAS	mcGAS	ccGAS	hcGAS	mcGAS	ccGAS
1							-	-	-	29	45	18
2							6	5	0	-	-	-
3	NH_2	NH_2	OH	H	OH	OH	90	54	47	0	31	0
4	NH_2	OH	OH	H	OH	OH	74	50	36	0	52	0
5	NH_2	F	H	OH	OH	OH	22	60	0	-	-	-
6	NH_2	Cl	H	H	OH	OH	0	29	0	-	-	-
7	SH	H	OH	H	OH	OH	78	73	19	-	-	-
8	Cl	H	H	H	OH	OH	0	0	0	-	-	-
9	$NHCH_3$	H	OH	H	OH	OH	67	91	9	-	-	-
10	SCH_3	H	OH	H	OH	OH	100	95	67	-	-	-
11	H	NH_2	OH	H	OH	OH	90	82	48	6	6	0
12	SH	NH_2	OH	H	OH	OH				0	0	0
13	Cl	NH_2	OH	H	OH	OH	91	100	71	0	5	0
14	OH	OH	OH	H	OH	OH	0	26	0	66	78	0
15	OH	H	OH	H	OH	OH	0	0	0	2	6	0
16	OCH_3	NH_2	OH	H	OH	OH	-	-	-	50	1	13
17	SCH_3	NH_2	OH	H	OH	OH	70	67	34	0	0	23
18	NH_2	H	H	OH	OH	OH	25	51	14	-	-	-
19	NH_2	H	H	F	OH	OH	0	0	0	-	-	-
20	NH_2	H	H	H	OH	OH	0	57	0	-	-	-
21	NH_2	H	NH_2	H	OH	OH	9	20	0	-	-	-
22	NH_2	H	F	H	OH	OH	0	38	0	-	-	-
23	NH_2	F	F	H	OH	OH	12	47	0	-	-	-
24	NH_2	H	Cl	H	OH	OH	0	0	0	-	-	-
25	NH_2	H	Br	H	OH	OH	0	0	0	-	-	-
26	NH_2	H	I	H	OH	OH	0	0	0	-	-	-
27	NH_2	H	OH	H	OCH_3	OH	0	0	0	-	-	-
28	OH	NH_2	OH	H	H	OH	-	-	-	0	17	0
29	OH	NH_2	OH	H	F	OH	-	-	-	3	72	34
30	OH	NH_2	OH	H	OH	SH	0	0	0	28	48	45
31	NH_2	H	OH	H	OH	SH	0	52	0	-	-	-

[a] 1mM ATP or GTP was reacted with 1mM NTP analogue in the presence of 5μM human, mouse or chicken full-length cGAS for 16 h at 37°C in 20μl volume. Reaction conversions were

determined by HPLC using UV detection at 260 nm. Conversions are defined as follows; a ratio of AUC of a CDN over the sum of AUCs of the CDN, NTPs and NDPs. - not determined.

As shown in Table 1A, N^1-methylguanosine-5'-triphosphate (**1**) was a mcGAS substrate but N^1-methyladenosine-5'-triphosphate (**2**) was not. Nucleotide triphosphates with 2-amino **(3),** 2-hydroxy **(4),** 2-fluoro (**5 and 23**), and 2-chloro (**6**) substitutions of adenosine were tolerated by mcGAS as well as NTPs with 6-mercaptopurine **(7),** 6-*N*-methyladenine **(9)** and 6-methylthiopurine **(10)** nucleobases; however, 2'-deoxy-6-chloropurine-5'-triphosphate (**8**) was not a mcGAS substrate. NTPs with 2-aminopurine **(11),** 6-thioguanine (**12**), 2-amino-6-chloropurine (**13**), xanthine (**14**), hypoxanthine (**15**) and 2-amino-6-methylthiopurine (**17**) nucleobases were

Table 1B. Substrate specificity of human, mouse and chicken cGAS toward NTP analogues.

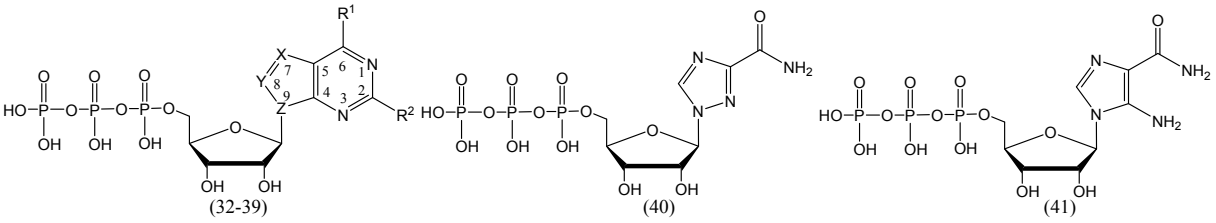

						Reaction Conversion (%)[a]					
						GTP			ATP		
NTP	R_1	R_2	X	Y	Z	hcGAS	hcGAS	ccGAS	hcGAS	hcGAS	ccGAS
32	NH_2	H	CH	CH	N	94	96	83	-	-	-
33	OH	NH_2	CH	CH	N	-	-	-	-	-	-
34	OH	NH_2	N-CH_3	CH	N	-	-	-	0	0	0
35	NH_2	H	N	N	N	29	58	24	-	-	-
36	NH_2	H	N	C-N_3	N	0	0	0	-	-	-
37	NH_2	H	N	C-OH	N	37	0	0	-	-	-
38	OH	NH_2	N	C-OH	N	-	-	-	0	0	0
39	OH	NH_2	C	CH	C	-	-	-	24	62	41
40						16	45	23	-	-	-
41						24	51	31	0	33	0

[a] 1mM ATP or GTP was reacted with 1mM NTP analogue in the presence of 5μM human, mouse or chicken full-length cGAS for 16 h at 37°C in 20μl volume. Reaction conversions were determined by HPLC using UV detection at 260 nm. Conversions are defined as follows; a ratio of AUC of a CDN over the sum of AUCs of the CDN, NTPs and NDPs. - not determined.

good mcGAS substrates. As mentioned above mcGAS did not tolerate O^6-methyl-guanosine-5'-triphosphate (**16**).

It was also possible to prepare CDNs by employing 7-deazaadenosine-5'-triphosphate **(32)** and 7-deazaguanosine-5'-triphosphate **(33)**, but not by the use of N^7-methylguanosine-5'-triphosphate **(34)** (Table 1B). 8-Azaadenosine-5'-triphosphate **(35)** was a substrate for mcGAS, but 8-azido-adenosine-5'-triphosphate **(36),** 8-oxo-adenosine-5'-triphosphate **(37)** and 8-oxo-guanosine-5'-triphosphate (**38**) were not. Interestingly, mcGAS could also catalyze synthesis of CDNs from thienoguanosine-5'-triphosphate **(39)**, ribavirin 5'-triphosphate **(40)** and 5-aminoimidazole-4-carboxamide-1-β-D-ribofuranosyl-5'-triphosphate (AICAR-5'-triphosphate) **(41)**.

Ara-adenosine-5'-triphosphate **(18),** 2'-deoxy-adenosine-5'-triphosphate **(20),** 2'-amino-2'-deoxy- **(21),** and 2'-fluoro-2'-deoxy-adenosine-5'-triphosphates **(22)** were also good mcGAS substrates; however, 2'-fluoro-2'-deoxy-*ara*-adenosine-5'-triphosphate **(19)**, 2'-chloro- **(24)**, 2'-bromo- **(25)**, and 2'-iodo-2'-deoxyadenosine-5'-triphosphates **(26)** were not accepted. Similarly, 3'-deoxy- **(28)** or 3'-fluoro- 3'-deoxy-guanosine-5'-triphosphate **(29)** were mcGAS substrates as were guanosine-5'-O-(1-thiotriphosphate) **(30)** and adenosine-5'-O-(1-thiotriphosphate) **(31)** (Table 1A).

Large scale synthesis of CDNs and profiling of their activity

Next, we initiated a larger scale synthesis of CDNs from NTP analogues. We attempted to prepare about 2 μmol of CDNs which was sufficient amount for their downstream biological and physico-chemical characterization. Some of the CDNs from nucleotide-5'-triphosphates listed in Tables 1A-1B could not be prepared in sufficient purity since nucleotide-5'-diphosphates or linear intermediates often co-eluted with CDNs. In the end, we prepared thirty-three CDNs enzymatically

and in order to get more complete SAR, we also prepared four CDNs (CDN-29, 35-37) through chemical synthesis (Table 2, 3, 4 and 6, for more details on synthesis of CDN-29, 35-37 see Supplementary Information).

To profile the activity of CDNs we employed cell based reporter assays. These assays are based on CDN/STING dependent expression of firefly luciferase from a reporter plasmid with four ISRE sites placed upstream of the firefly luciferase reporter gene minimum promoter. The luciferase expression is induced by IRF3 transcription factor as a result of STING signaling cascade activation.[32] We have developed the reporter assays for five STING haplotypes that are present in humans[33] and run them in two assay formats. In digitonin assay we performed permeabilization of cellular membranes with a detergent (digitonin A). As a consequence, the uptake of negatively charged CDNs into cells was not the limiting step in STING activation. In standard assay, the detergent was absent and the activity of CDNs was therefore influenced by efficiency of their cellular uptake. Finally, our biochemical assay (differential scanning fluorimetry, DSF) determined difference between melting temperature of STING protein with and without ligand (ΔT_m) and was an indirect measure of CDNs binding affinity to STING protein. ΔT_m values from the DSF assay correlated better with log EC_{50} values from digitonin (Pearson r = -0.73, P (two-tailed) < 0.0001) than with log EC_{50} values from standard assay (Pearson r = -0.56, P (two-tailed) 0.001) (SI Figure S1). EC_{50} values were calculated from dose response curves of individual CDN treated cells in digitonin or standard assay. Representative dose response curves are shown in Figure S2. To compare results of presented cell-based and biochemical assays for all prepared CDNs see Table 2, 3, 4, and 6.

Structure and conformation of CDNs in water solution.

All prepared CDNs (CDN 1 – 37) were characterized by ^{1}H, ^{31}P and ^{19}F NMR spectra and high-resolution MS. The NMR data are summarized in Tables S1a, S1b, S2, S3, S4, S5. ^{31}P chemical shifts clearly distinguished the presence of thiophosphate group (δ 52-57 ppm in CDNs 33 – 37) from phosphate group (δ +1.5 to -1.5 ppm in all other CDNs 1 - 32). ^{19}F signals in the range δ -196 to -200 ppm proved fluorine substituent on furanose ring (CDNs 1 – 8) while signal around δ -50 showed CDNs with fluorine substituent in position 2 of nucleobase (CDNs 6 and 7). Basic conformation features of CDNs can be derived from vicinal coupling constants and observed homonuclear NOEs. Furanose rings of CDNs with ribose sugar units and a 2'-phosphate group adopted *C2'-endo* conformation (characterized by large J(1',2') = 7 – 9 Hz and small J(3',4') = 0 - 1.5 Hz) while rings with 3'-phosphate group preferred *C3'-endo* conformation (manifested by very small J(1',2') = 0 – 1.5 Hz and large J(3',4') = 7 - 9 Hz). Orientation of the nucleobase was found as *anti*- throughout the whole series of our CDNs as indicated by characteristics observed from NOE contacts: between H-8 and protons H-1', H-2' in 2'-phospate units and between H-8 and protons H-1', H-2', H-3' in 3'-phosphate units. The structure modifications of the nucleobase had only a very small effect on the conformation of furanose ring. For conformation analysis of phosphate and thiophosphate linkages of CDNs there was not a complete set of proper NMR parameters accessible. While torsion angles β and ε were still related to vicinal heteronuclear couplings J(P,H) observable in ^{1}H NMR spectra and J(P,C) obtainable from ^{13}C NMR spectra, for torsion angles α and ζ such usable couplings were missing.

2' and 3' substituted 2'3'CDNs

We were able to prepare fifteen 2'3'CDNs with substitutions at 2'-position of adenosine or 3'-position of guanosine monophosphate units (Table 2). Compared to the parent 2'3'cGAMP, all but one CDNs (CDN-11) had less than five-fold shift in EC_{50} values in the digitonin reporter assay using cells expressing WT, HAQ and AQ STING haplotypes (Table 2). The important difference appeared in the case of REF STING haplotype that is present in about 13% of humans.[33,34] 2'3'CDNs with 2'-amino-2'-deoxyadenosine (CDN-9), *ara*-adenosine (CDN-10), and some with deoxyribonucleotides (CDN-13, -14) were at least 10-fold less active against REF than WT STING haplotype (Table 2). Similarly, fluoro- (CDN-6, CDN-11) or chloro- (CDN-15) substitutions at C_2 position of adenine resulted in decreased activity against the REF STING.

Despite log EC_{50} values from digitonin and ΔT_m values from DSF assay correlated well (Figure S1), clear outliers could be found (e.g. CDN-1 and -2 vs 2'3'cGAMP). This is probably due to differences in efflux and/or intra/extracellular stability of these CDNs that are captured in digitonin cell-based assay but not in DSF assay.

We also determined activities of the prepared CDNs in the standard assay using WT STING 293T reporter cells (Tables 2, 3, 4, 6). Due to the dramatic effect of the cellular uptake on the activity of CDNs, EC_{50} values for all prepared CDNs were more than 100-fold higher compared to EC_{50} values from the digitonin assay (Tables 2, 3, 4, 6).

Throughout the study, we attempted to explain all experimentally observed binding affinities of CDNs with STING by employing crystallography and computational modelling. For relative comparison of binding affinity of CDNs to STING, we used ΔT_m values from our biochemical DSF assay. In order to highlight changes brought about by individual modifications of a ligand we discuss $\Delta\Delta T_m$, defined as the difference between ΔT_m of a ligand X and a reference ligand specified

in the text below. Positive values of $\Delta\Delta T_m$ (X) indicate higher stability of protein-ligand complex than in the case of a reference ligand.

Table 2. Activity of 2'OH and 3'OH substituted 2'3'CDNs in biochemical and cell-based assays.

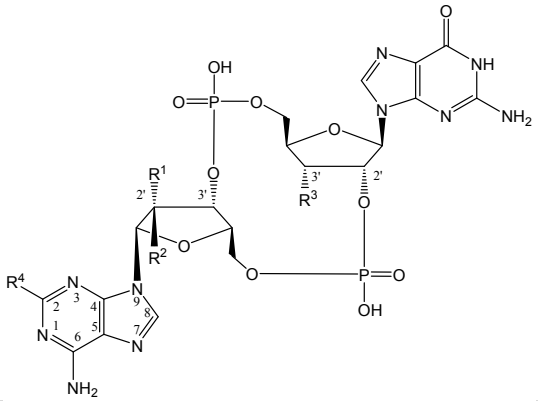

					DSF	STANDARD ASSAY	DIGITONIN ASSAY				
					ΔT_m (°C)[a]	EC_{50} (μM) [b]	EC_{50} (μM) [c]				
Compound	R_1	R_2	R_3	R_4	WT	WT	WT	HAQ	REF	AQ	Q
CDN-1	F	H	OH	H	20.5	13.8	0.01	0.01	0.01	0.03	0.02
CDN-2	F	H	F	H	20.3	13.3	0.02	0.05	0.02	0.09	0.20
CDN-3	OH	H	F	H	16.2	16.7	0.02	0.02	0.07	0.01	0.04
CDN-4	F	H	H	H	17.4	10.7	0.02	0.05	0.04	0.04	0.18
CDN-5	H	H	F	H	16.6	15.1	0.01	0.04	0.07	0.02	0.06
CDN-6	H	H	F	F	10.7	>300	0.05	0.10	2.00	0.17	0.70
CDN-7	F	H	OH	F	14.7	11.0	0.02	0.08	0.07	0.03	0.08
CDN-8	F	H	OH	NH_2	14.4	27.6	0.02	0.04	0.17	0.03	0.13
CDN-9	NH_2	H	OH	H	9.4	107.5	0.02	0.03	1.40	0.02	0.24
CDN-10	H	OH	OH	H	17.0	nd	0.04	0.08	0.40	0.04	0.09
CDN-11	H	OH	OH	F	12.3	186.8	0.20	0.1	6.40	0.06	0.60
CDN-12	H	H	OH	H	15.8	31.9	0.02	0.06	0.14	0.03	0.34
CDN-13	H	H	H	H	13.5	75.4	0.06	0.03	3.30	0.03	0.04
CDN-14	OH	H	H	H	13.2	21.6	0.01	0.03	0.40	0.03	0.12
CDN-15	H	H	OH	Cl	9.5	58.2	0.07	0.08	4.70	0.09	0.96
2'3'-cGAMP					15.3	13.7	0.02	0.02	0.07	0.04	0.05
2'2'-cGAMP					11.6	39.2	0.03	0.02	0.21	0.03	0.17
3'3'-cGAMP					5.1	70.1	0.12	0.12	4.30	0.26	2.06
3'3'c-diAMP					2.5	14. 9	0.3	0.2	>45	0.2	7.1
3'3'c-diGMP					2.4	184.2	4.5	0.9	8.40	1.1	>45

[a] Results of differential scanning fluorimetry assay performed with WT STING haplotype. ΔT_m values are the mean of two independent double determinations. [b] Results of standard assay in 293T reporter cells expressing WT STING haplotype. [c] Results of digitonin assay in 293T reporter cells expressing different STING haplotypes. EC_{50} values are the mean of two independent experiments measured in triplicates with standard deviations <50% of EC_{50} values.

Several modifications of the sugar ring on both nucleotides have been examined. For the 3' nucleotide, these modifications include substitution of the 2'-hydroxyl with 2'-fluorine (CDN-1), hydrogen (i.e. deoxyribose, CDN-12), amine group (CDN-9), or changed stereochemistry of 2' carbon (i.e. arabinose, CDN-10).

Of these modifications, CDN-9 forms the least stable ligand-protein complex. The amine group of the unbound ligand is expected to be protonated. However, it is improbable that the binding site would favor presence of a positively charged substituent. Thus, binding of this ligand is expected to incur a desolvation penalty, which in turn leads to decreased thermal stability of the protein-ligand complex (ΔT_m(CDN-9) = +9.4 ºC, i.e. $\Delta\Delta T_m$ = -5.9 ºC with respect to 2'3'cGAMP (see Table 2)).

According to QM/MM models, the arabinose modification (CDN-10) is accommodated by the 2' hydroxyl interaction with Arg238. This differs from 2'3'cGAMP-STING complex where this amino acid is primarily in contact with the phosphate group.[8] In the case of CDN-10 the phosphate is displaced and interacts with Arg232 and the 2' hydroxyl via intramolecular hydrogen bonding. Thus, the arabinose modification is well tolerated by WT STING which is reflected by $\Delta\Delta T_m$(CDN-10) = +1.7 ºC with respect to 2'3'cGAMP .

In the crystal structure of 2'3'cGAMP with STING, the environment surrounding 2'-hydroxyl includes both hydrophobic and hydrophilic residues and a nearby water molecule (Figure 1). The amphipathic character of this region contributes to the ability of the protein to accommodate less hydrophilic substitutions of 2'-hydroxyl, e.g. hydrogen (i.e. deoxyribose, $\Delta\Delta T_m$(CDN-12) = + 0.5 ºC or fluorine, $\Delta\Delta T_m$(CDN-1) = +5.2 ºC, both in respect to 2'3'cGAMP). On the other hand, the environment around the 3'-hydroxyl of the 2'-nucleotide is significantly more hydrophilic. Thus, these same modifications (i.e. hydrogen or fluorine substitution in the 3'-position of the

2'-nucleotide) are less favorable than their 2'-position counterparts, with $\Delta\Delta T_m$(CDN-3) = +0.9 ºC and $\Delta\Delta T_m$(CDN-14) = -1.8 ºC compared to 2'3'cGAMP (Table 2).

While the above explanations help to rationalize some of the observed differences, it is remarkable that the 2'-fluorine (CDN-1) and arabinose (CDN-10) modifications actually lead to higher ΔT_m with respect to the native ligand. One can speculate that this improvement in STING binding is not due to their specific interaction with the protein but an inherently lower energetic cost for these ligands to adapt the STING bound conformation.

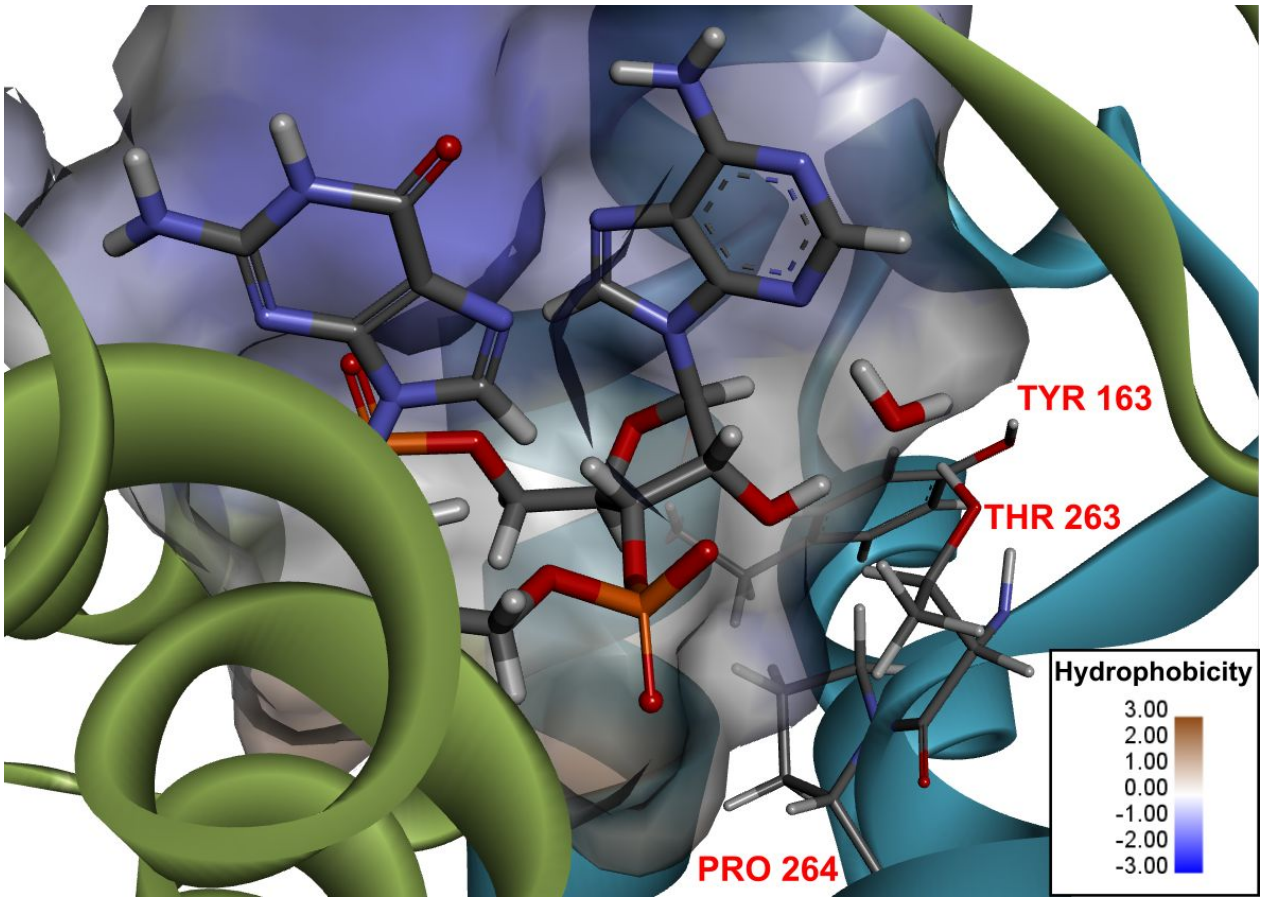

Figure 1. Amphipathic pocket around the 2' position of 3' nucleotide.

The environment includes both hydrophobic (Tyr163 and Pro264) and hydrophilic residues (Thr263) and a water molecule. Hydrophobicity visualized by BIOVIA Discovery Studio[35]. Structure obtained from a QM/MM model based on PDB 6T1X. Only the relevant residues and the ligand are shown in stick representation.

By combining QM/MM models and conformational sampling of these two ligands we can estimate this energetic penalty (see methods). Indeed, it turns out that both CDN-1 and CDN-10 require 4.7 and 4.6 kcal.mol^{-1} less of (free) energy, respectively, than 2'3'cGAMP to change the conformation from unbound state in solvent to that found in the protein. These estimates are qualitative but serve to illustrate that the ligand may be optimized not only by its interactions with the protein but also via minimizing its conformational strain.

The 2'- and 3'-hydroxyl groups of the native ligand are more than 7 Å apart. Based on the crystal structure of CDN-1 with WT STING, substituting 2' hydroxyl with fluorine does not lead to any significant change in the binding mode. We presume the same is the case for substitution with hydrogen (CDN-12) and analogous substitutions of the 3' hydroxyl (CDN-3 and CDN-14). Thus, it is not surprising that combined modifications result in additive changes of $\Delta\Delta T_m$. Indeed, measurement of $\Delta\Delta T_m$ for disubstituted ligands CDN-2, CDN-4, CDN-5 and CDN-13 give values that can also be estimated by simply summing up the $\Delta\Delta T_m$ values of monosubstituted ligands. The error of such estimate is within 1.1 ºC, which is within the 3 times standard deviation of DSF measurement. Further examples of such additivity or lack thereof will be discussed below and may be used as an argument for cooperative effects of substitutions in different parts of a ligand.

2'3'CDNs with substituted nucleobases

2'3'CDNs with guanosine subunit combined with 2-aminoadenosine (CDN-16), N^6-methyladenosine (CDN-17), inosine (CDN-18), 2-aminopurineriboside (CDN-21) or 7-deazaadenosine (CDN-24) (Table 3), and 2'3'CDNs with adenosine subunit combined with N^1-methylguanosine (CDN-28), inosine (CDN-29), 7-deazaguanosine (CDN-30), and thienoguanosine (CDN-31) (Table 4) retained comparable activities in WT, HAQ and AQ STING digitonin reporter assays as 2'3'cGAMP. Compared to 2'3'cGAMP, 2'3'CDN with xanthosine-

MP (CDN-19), 6-thio-IMP (CDN-20), 6-methylthio-GMP (22), 8-aza-AMP (CDN-25) and AICAR-MP (CDN-26 and -32) had substantially diminished activity against all STING haplotypes (Table 3 and 4). Moreover, with exemption of CDN-29, all prepared 2'3'CDNs had significantly impaired activity toward REF STING haplotype in digitonin assays (Table 3 and 4). Similar to 2' and 3' substituted 2'3'CDNs, CDN-16 to 32 were at least two order of magnitude less potent in standard than digitonin assay (Table 3 and 4).

Table 3. Effects of nucleobase modifications at 3'-nucleotide on CDN activity in biochemical and cell-based assays.

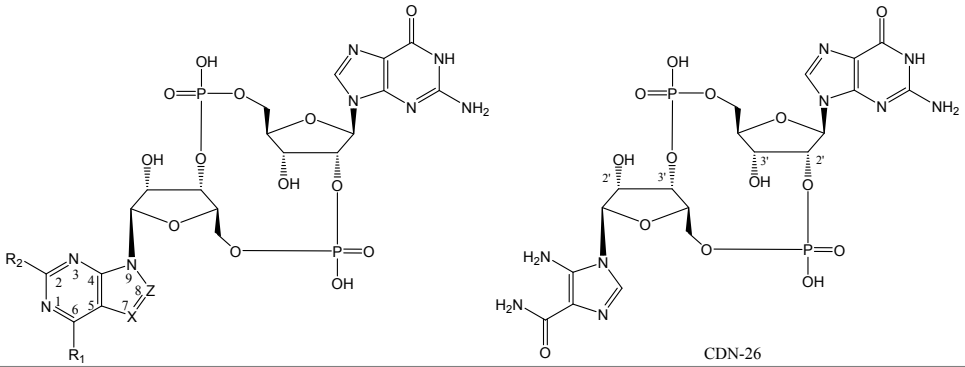

CDN-26

					DSF	Standard Assay	Digitonin Assay				
					ΔT_m (°C) [a]	EC_{50} (μM) [b]	EC_{50} (μM) [c]				
Compound	R_1	R_2	X	Z	WT	WT	WT	HAQ	REF	AQ	Q
CDN-16	NH_2	NH_2	N	CH	10.0	35.9	0.02	0.05	1.10	0.04	0.31
CDN-17	$NHCH_3$	H	N	CH	9.0	63.7	0.02	0.06	0.70	0.06	1.20
CDN-18	OH	H	N	CH	8.8	148.8	0.05	0.30	2.10	0.14	2.20
CDN-19	OH	OH	N	CH	2.4	>300	1.80	1.70	20.9	2.00	32.8
CDN-20	SH	H	N	CH	7.3	182.1	0.30	0.20	1.70	0.15	8.30
CDN-21	H	NH_2	N	CH	9.2	53.9	0.02	0.04	1.60	0.04	0.70
CDN-22	SCH_3	NH_2	N	CH	3.5	>300	0.30	0.48	27.6	0.24	8.50
CDN-23	SCH_3	H	N	CH	8.3	13.3	0.01	0.06	2.30	0.06	1.23
CDN-24	NH_2	H	CH	CH	11.5	66.4	0.01	0.02	0.28	0.01	0.16
CDN-25	NH_2	H	N	N	3.9	>300	0.23	0.31	34.2	0.21	5.72
CDN-26					1.7	>300	0.32	0.21	>45	0.21	45.3
2'3'-cGAMP					15.3	13.7	0.02	0.02	0.07	0.04	0.05

[a] Results of differential scanning fluorimetry assay performed with WT STING haplotype. ΔT_m values are the mean of two independent double determinations. [b] Results of standard assay in 293T reporter cells expressing WT STING haplotype. [c] Results of digitonin assay in 293T reporter cells expressing different STING haplotypes. EC_{50} values are the mean of two independent experiments measured in triplicates with standard deviations <50% of EC_{50} values.

CDNs are anchored to STING protein through Arg238 and Tyr167 which stack via π - π and cation - π interactions from both sides of nucleobases (Figure 2). The functional groups at C_6 position on CDNs are without direct contacts with the protein. Instead, their interactions with STING are mediated through a network of water molecules to backbone groups of residues 238 to 241, which are located in the lid region (Figure 3) of STING protein. This water network might be crucial for understanding the effect of base modification on the activity of CDNs.

Table 4. Effects of nucleobase modifications at 2'-nucleotide on CDN activity in biochemical and cell-based assays.

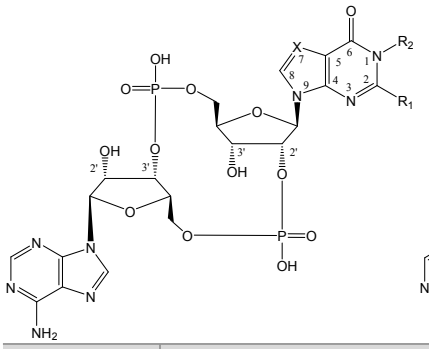

CDN-31

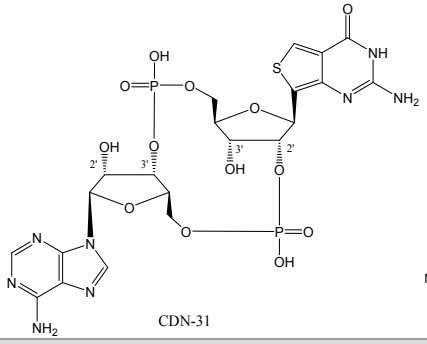

CDN-32

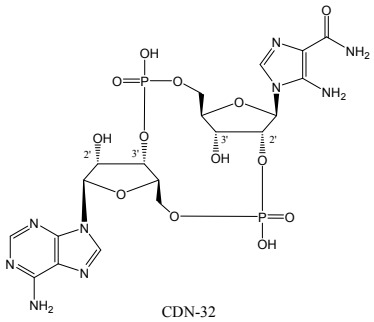

				DSF	Standard Assay	Digitonin Assay				
				ΔT_m (°C) [a]	EC_{50} (μM) [b]	EC_{50} (μM) [c]				
Compound	R_1	R_2	X	WT	WT	WT	HAQ	REF	AQ	Q
CDN-27	OH	H	NH	7.6	>300	0.13	0.19	5.80	0.18	0.72
CDN-28	NH_2	CH_3	NH	9.0	40.0	0.02	0.04	0.90	0.04	0.78
CDN-29	H	H	NH	16.1	29.9	0.02	0.03	0.04	0.01	0.02
CDN-30	NH_2	H	CH	6.6	40.4	0.04	0.10	3.50	0.06	1.10
CDN-31				2.8	240.6	0.11	0.25	6.00	0.05	3.00
CDN-32				0.6	>300	0.83	0.40	>45	0.42	47.20
2'3'-cGAMP				15.3	13.7	0.02	0.02	0.07	0.04	0.05

[a] Results of differential scanning fluorimetry assay performed with WT STING haplotype. ΔT_m values are the mean of two independent double determinations. [b] Results of standard assay in 293T reporter cells expressing WT STING haplotype. [c] Results of digitonin assay in 293T reporter cells expressing different STING haplotypes. EC_{50} values are the mean of two independent experiments measured in triplicates with standard deviations <50% of EC_{50} values.

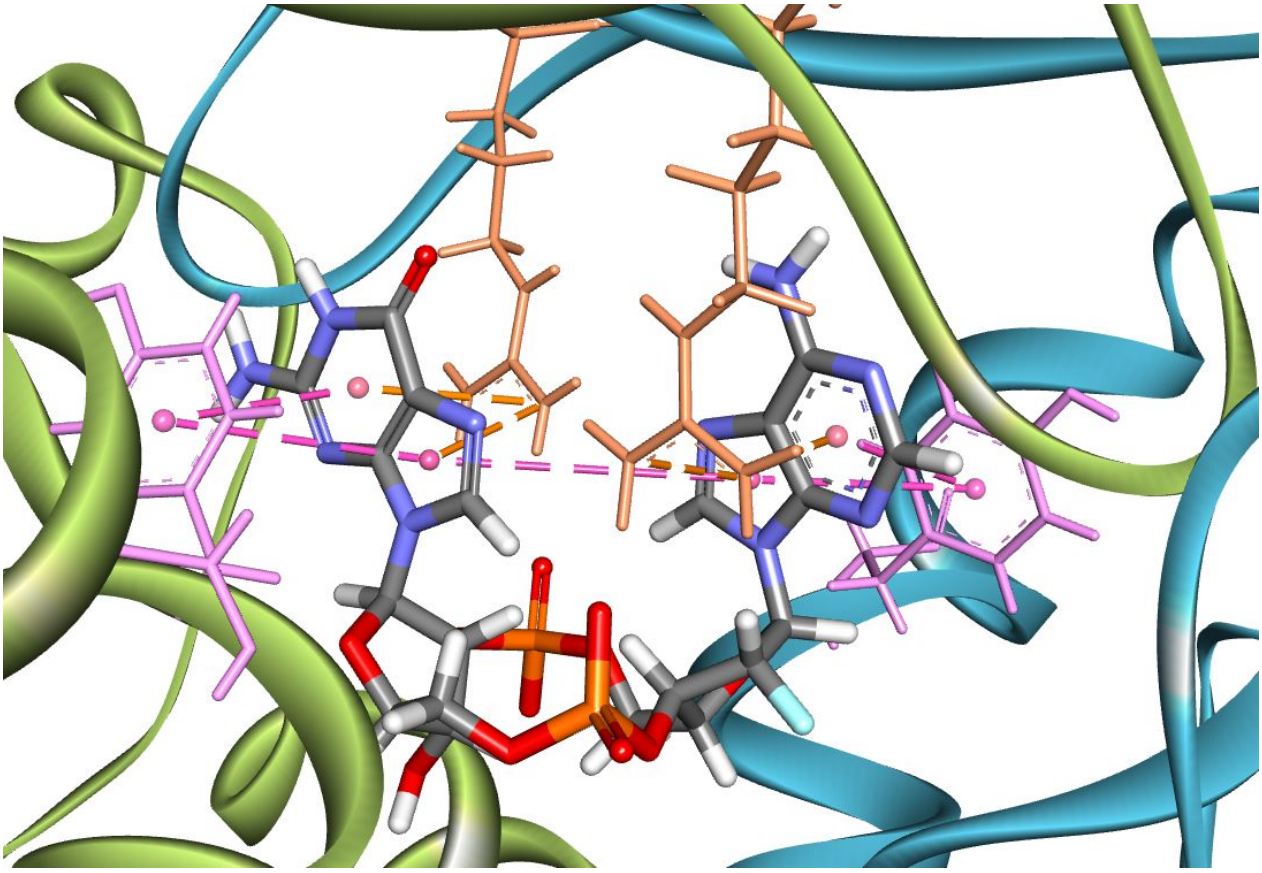

Figure 2: Interactions of purine bases.
Purine bases of a CDN stack with Tyr167 and Arg238 residues. Detail from the structure of CDN-1 with human WT STING (PDB: 6S27). The π -π interaction shown in dashed-pink line and cation-π interaction shown in dashed-orange line, respectively.

Information about the positions of water molecules is difficult to interpret due to symmetry considerations. A 2'3' cyclic dinucleotide allows for two equivalent binding modes to a symmetric STING homodimer. Even if the water molecules are resolved in a crystal structure, the averaging of their positions poses a challenge for a fundamentally asymmetric ligand interpretation. In the following, we rely on the ability of QM/MM calculations to provide detailed structural information concerning water positions. Moreover, most of the ligands presented herein contain modification of the adenine base (with respect to the native 2'3'cGAMP ligand) and hence, the discussion of water environment is focused on this region.

Figure 3 shows the proposed network of water molecules. This configuration not only provides an ideal number of interactions for all water molecules in the network, but also accommodates the asymmetry of the ligand, i.e. hydrogen bond acceptor at position 6 of guanine and hydrogen bond donor at position 6 of adenine. This configuration agrees well with water molecules resolved in a crystal structure of STING in complex with CDN-24. There is one less water molecule in the QM/MM model in the vicinity of position 2 of 3' nucleotide due to a different orientation of Ile235 side-chain in the crystal structure and in the QM/MM model.

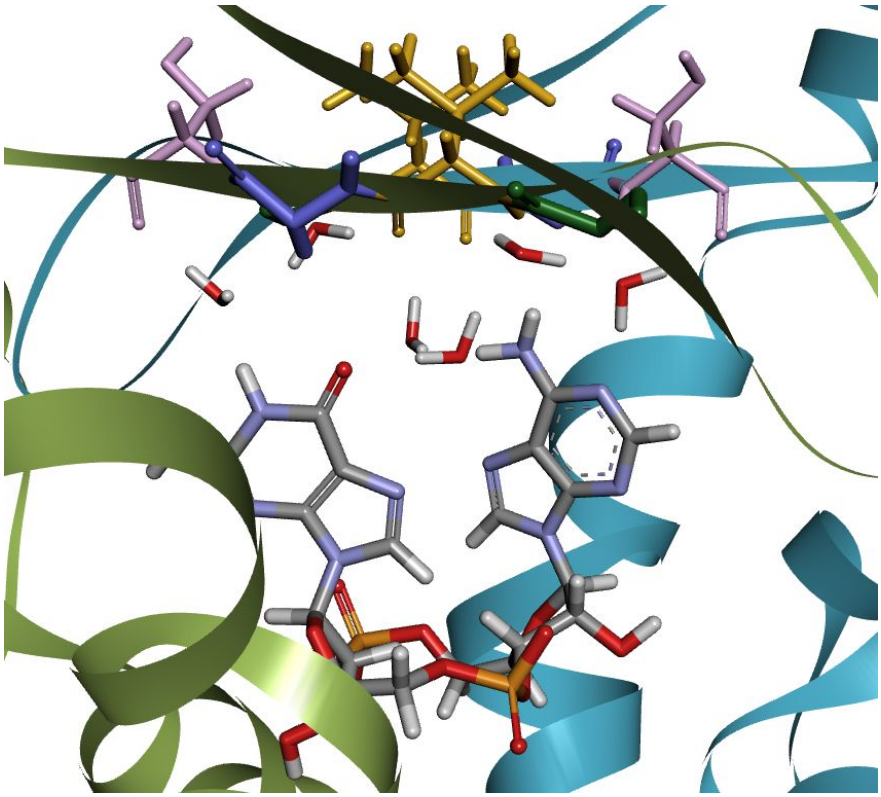

Figure 3. Proposed local water network near positions 6 of 2'3cGAMP.

Water-mediated hydrogen bond network between the purine bases of 2'3'cGAMP and the lid region backbone groups of residues 238 (green), 239 (yellow), 240 (purple), and 241 (pink) located in β3/ β4 strands of human WT STING's lid domain. Four water molecules together with position 6 substituents of purine bases form an asymmetrical chain of hydrogen donors and acceptors. Structure was obtained from a QM/MM model based on PDB 6T1X. Only the relevant residues and the ligand are shown in stick representation.

We speculate that this ideal setup is sensitive to modification of nearby functional groups. Changing a substituent at the position 6 of adenine to an electron acceptor, such as oxygen (CDN-18) or sulfur (CDN-20), leads to ΔΔTm ≈ -7 ºC with respect to 2'3'cGAMP. Bulkier substituents like 6-methyl-amino (CDN-17) and 6-methylthio (CDN-23) are also disruptive, probably due to the decreasing number of water molecules around these ligands. Regardless of the nature of the methylated substituent, this disruption also leads to $\Delta\Delta T_m \approx$ -7 ºC. On the other hand, substitution of NH_2 group with hydrogen is accommodated without incurring a penalty to ΔT_m (compare CDN-16 and CDN-21).

Shifting the focus to substitutions on position 2, it seems that any substituent other than the native hydrogen incurs a penalty of a $\Delta\Delta T_m \approx$ -5 ºC relative to an unsubstituted CDN, as evidenced by a number of cases, including amine substitutions (compare ΔT_m values of CDN-16 and 2'3'cGAMP; CDN-22 and CDN-23; CDN-1 and CDN-8), oxygen (compare ΔT_m values of CDN-18 and CDN-19), fluorine (compare ΔT_m values of CDN-10 and CDN-11, CDN-1 and CDN-7, CDN-5 and CDN-6), and chlorine (CDN-15 and CDN-12).

Note the approximate penalties mentioned in the previous paragraphs, i.e. $\Delta\Delta T_m \approx$ -7 ºC for an electron acceptor or methylated substituent in position 6 and $\Delta\Delta T_m \approx$ -5 ºC for any substituent at position 2 of the 3' nucleotide. These two very simple rules are sufficient to estimate measured ΔT_m of all 14 ligands with substituted purine base of 3' nucleotide in our set for which ΔT_m span from +2.4 to +14.9 ºC to within 1.3 ºC (with mean absolute deviation of 0.7 °C), which is well within the experimental error. The above QSAR analysis is summed up in Table 5.

Table 5. QSAR of ligand modifications.

Position	Native substituent	Modified substituent	DSF[a] $\Delta\Delta T_m$ (^{O}C)
6 (3'nucleotide)	NH_2	Hydrogen-bond acceptor	-7
6 (3'nucleotide)	NH_2	methylated	-7
2 (3'nucleotide)	H	any	-5
2' (3'nucleotide)	OH	F	+5
2' (3'nucleotide)	OH	H	+0.5
3' (2'nucleotide)	OH	F	+1
3' (2'nucleotide)	OH	H	-2

[a] $\Delta\Delta T_m$, defined as the difference between ΔT_m of a ligand X and reference ligand.

Thiophosphate 2'3'CDNs

We were able to prepare enzymatically two thiophosphate 2'3'CDNs. Mono-thiophosphate 2'3'CDN (CDN-33) is about 3-7-fold less active against all STING haplotypes than 2'3'cGAMP. On the other hand, bis-thiophosphate CDN (CDN-34) retains similar activity toward all STING haplotypes as the parent 2'3'cGAMP (Table 6). Since the enzymatic cyclization afforded only one diastereomer out of four possible, we prepared bis-thiophosphate versions of 2'3'cGAMP through chemical synthesis, which is detailed in Supplementary Methods. As shown in Table 6, none of the prepared compounds had activity profile similar to the enzymatically prepared CDN-34. Moreover, ^{1}H-NMR data of CDN-34 differed from those for the chemically prepared diastereomers CDN-35, -36 and -37, indicating that CDN-34 is the diastereomer which was not obtained during chemical synthesis of CDN-35, -36 and -37.

Table 6. The activity of thiophosphate 2'3'CDNs in biochemical and cell-based assays.

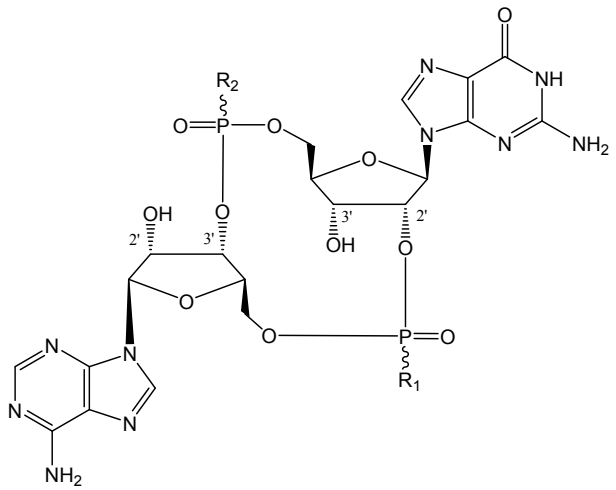

Compound	R_1	R_2	DSF ΔT_m (°C) [a] WT	Standard Assay EC_{50} (μM) [b] WT	Digitonin Assay EC_{50} (μM) [c] WT	HAQ	REF	AQ	Q
CDN-33	OH	SH	13.8	nd	0.06	0.11	0.6	0.12	0.14
CDN-34	SH	SH	14.6	70.7	0.03	0.02	0.01	0.03	0.03
CDN-35	SH	SH	13.6	7.0	0.09	0.13	0.7	0.14	0.19
CDN-36	SH	SH	15.1	120.6	0.02	0.02	0.2	0.03	0.07
CDN-37	SH	SH	14.8	1.0	0.03	0.03	0.15	0.03	0.08
2'3'-cGAMP			15.3	13.7	0.02	0.02	0.07	0.04	0.05

[a] Results of differential scanning fluorimetry assay performed with WT STING haplotype. ΔT_m values are the mean of two independent double determinations. [b] Results of standard assay in 293T reporter cells expressing WT STING haplotype. [c] Results of digitonin assay in 293T reporter cells expressing different STING haplotypes. EC_{50} values are the mean of two independent experiments measured in triplicates with standard deviations <50% of EC_{50} values.

QM/MM modelling of CDN-34 and its diastereoisomers (CDN-35, CDN-36, and CDN-37) reveals very few differences. The native ligand (phosphate) and R configuration of the thiophosphate exhibit identical binding modes. In case of S-configuration of the thiophosphate (i.e. P=S bond pointing in direction of Arg238), the interaction is shared with both Arg232 and Arg238. Hence, we speculate that (S,S) configuration is the one that would be most affected in REF variant of the protein (i.e. R232H allelic form). However, this difference alone is not sufficient for explaining all the observed differences in activities.

The structures of WT STING with CDN-1 and -24

By employing our optimized protocol[36], we were able to obtain crystal structures of human WT STING in complex with CDN-1 and -24 with final resolutions of 3Å (I/σ = 2) and 2.2Å (I/σ = 2), respectively. The crystal of STING in complex with CDN-1 belonged to the tetragonal $P4_12_12$ and in complex with CDN-24 to the orthorhombic $P2_12_12$ space group (Tables S6 and S7). The alignment of the structure of the WT STING in complex with CDN-1 or CDN-24 with structure of STING in complex with 2'3'cGAMP (PDB entry 4KSY) revealed slight differences in protein

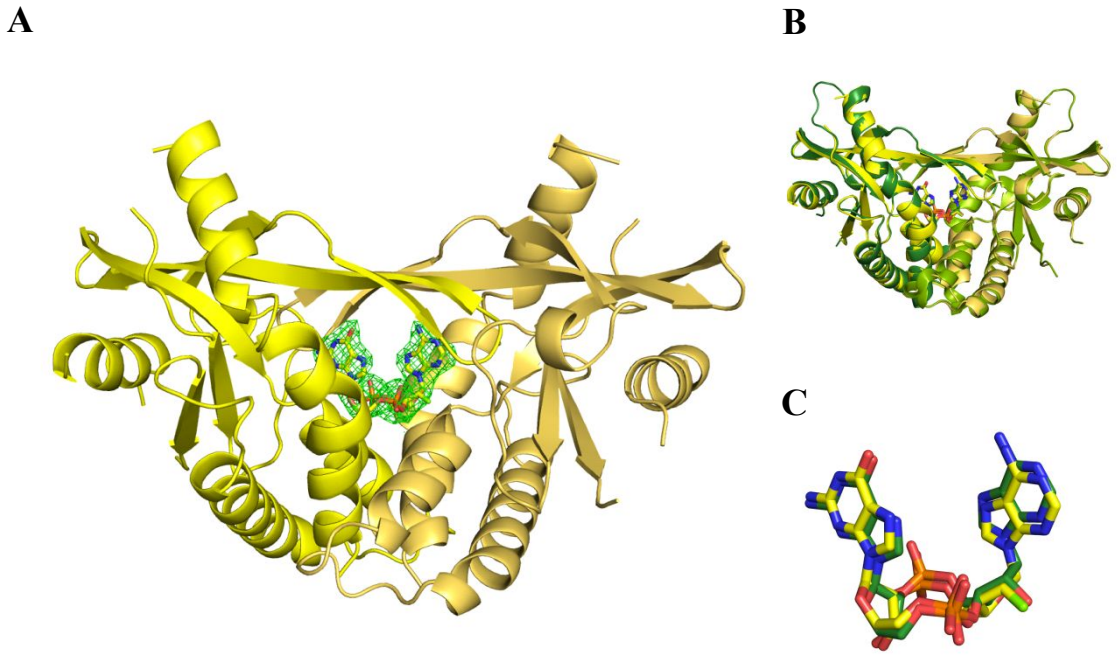

Figure 4. Structure of human WT STING in complex with CDN-1 (6S27) and its comparison to the structure of STING in complex with its natural ligand 2'3'cGAMP (4KSY).

A) Structure of human WT STING in complex with CDN-1 (6S27). The Fo-Fc map is contoured at I/σ = 3. B) Alignment of 6S27 and 4KSY (the RMSD over C-alpha = 0.5690). C) Comparison of 2'3'-cGAMP and CDN-1 bound to the STING. Coloring: Nitrogen – blue, Oxygen – red, Fluorine – bright green, Phosphate – orange, Carbon – yellow (CDN-1) or dark green (2'3'cGAMP).

conformation (the RMSD over C-alpha 0.57 and 0.78, respectively) and the protein structures can be therefore considered virtually identical (Figure 4B and 5B). The binding mode and conformation of the CDN-1 and CDN-24 correspond well to the binding mode and conformation of 2'3'-cGAMP (Figure 4C and 5C).

The water network chain in the vicinity of position 6 of purine bases coincides with those used in QM/MM calculation, which *a posteriori* confirms the validity of our previous structural considerations on water networks. However, compared to QM/MM model, both X-ray structures show an extra water molecule near position 1 due to different orientation of Ile235 side-chain. Also, both crystal structures lack one water molecule near position 3 (Figure 3).

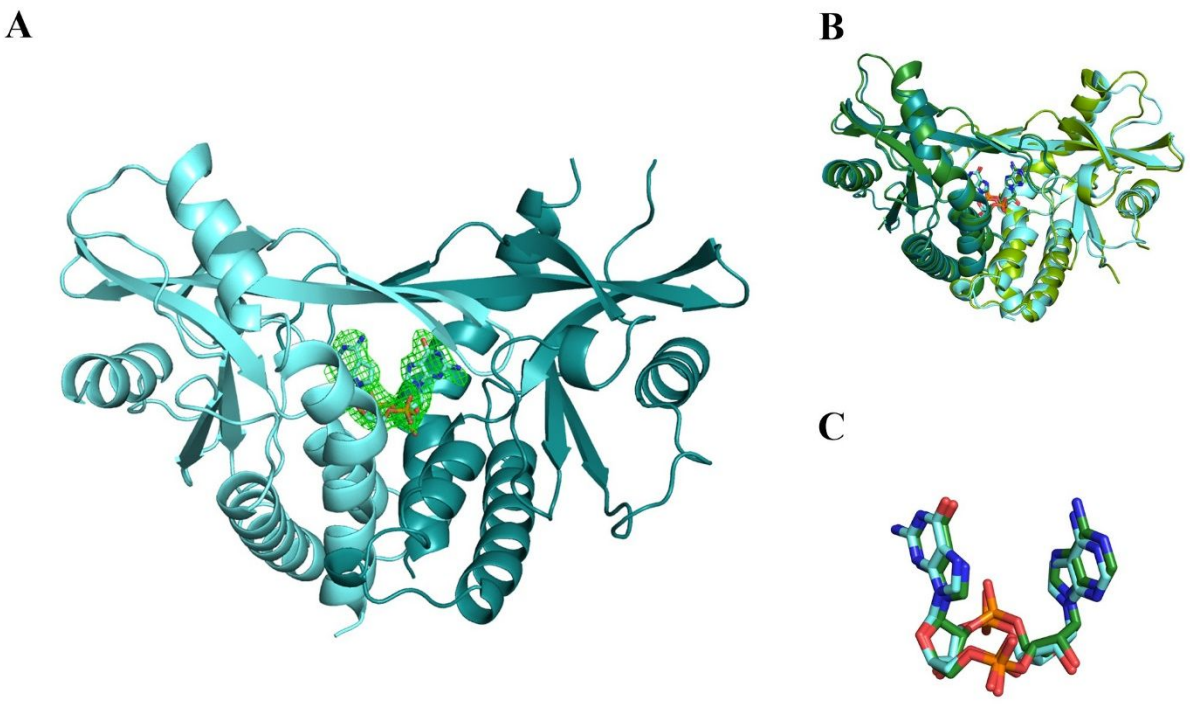

Figure 5. Structure of human WT STING in complex with CDN-24 (6S26) and its comparison to the structure of STING in complex with its natural ligand 2'3'cGAMP (4KSY).

A) Structure of human WT STING in complex with CDN-24 (6S26). The Fo-Fc map is contoured at I/σ = 3. B) Alignment of 6S26 and 4KSY (the RMSD over C-alpha = 0.7833).

C) Comparison of 2'3'-cGAMP and CDN-24 bound to the STING. Coloring: Nitrogen – blue, Oxygen – red, Phosphate – orange, Carbon – light blue (CDN-24) or dark green (2'3'cGAMP).

Effect of 2'3'CDNs on cytokine induction and monocytes

Activation of cGAS-STING pathway results in the induction of interferons and TNF secretion.[37] Consistently, PBMC treated with CDNs prepared within this study induced high level of IFNα, IFNγ and TNFα secretion into cultivation medium (Table 7, Table S8). Since CDNs were reported to induce monocytic cytotoxicity in A2a Gαs Protein-Coupled Receptor dependent manner,[37] we tested the effect of CDNs 1 - 37 on viability of monocytes in PBMC using a single concentration of 12.5μM. Similar to the published data, the majority of the prepared compounds caused profound monocytic cytotoxicity without affecting $CD3^+$ T cell population (Table 7, Table S8).

Table 7. Effect of CDNs on monocyte viability and cytokine induction in PBMC assay.

Compound	Monocyte viability [a]	Cytokines (fold of 2'3'cGAMP induced cytokines)[b]		
		INF γ	TNF α	IFN α
CDN-1	1.7%	1.3	0.6	0.9
CDN-2	0.4%	5.1	4.3	0.5
CDN-3	0.7%	4	0.8	0.6
CDN-4	0.7%	6.2	4.4	0.3
CDN-5	0.5%	5.6	4.2	0.3
CDN-6	0.2%	0.1	2.3	0
CDN-7	0.4%	4.6	3.2	0.4
CDN-8	2.5%	3.1	0.7	0.8
CDN-9	3.0%	2.7	3.7	0.4
CDN-10	5.2%	3.2	2.6	1
CDN-11	3.0%	3.2	3.4	2.4
CDN-12	2.3%	3.3	4.1	0.5
CDN-13	1.6%	1.6	0.6	1.3
CDN-14	3.3%	5	1.9	0.6
CDN-15	0.1%	0.8	4.3	0.1
CDN-16	1.5%	3.6	4.3	0.7
CDN-17	0.8%	3.3	4.1	0.5
CDN-18	17%	0.5	0.2	0.8

CDN-19	45%	0	0	0
CDN-20	10%	1.8	0.7	0.7
CDN-21	0.6%	2.4	4.1	0.5
CDN-22	4.8%	1.1	3.2	0
CDN-23	0.4%	1.7	4.2	0.2
CDN-24	0.7%	1.2	3.3	0.3
CDN-25	2.3%	2.9	3.8	0.1
CDN-26	83%	0	0	0
CDN-27	8.3%	3	0.6	0.7
CDN-28	2.0%	3.3	0.5	0.7
CDN-29	1.0%	1.2	0.4	1.9
CDN-30	0.9%	5.9	3.5	0.3
CDN-31	0.9%	4	1.6	2.4
CDN-32	87%	0	0	0
CDN-33	9.4%	2.2	1.6	1.2
CDN-34	2.1%	2.4	1.3	2
CDN-35	1.8%	1	0.2	0.6
CDN-36	0.3%	3.9	0.4	1.2
CDN-37	0.8%	0.2	0.5	0.1
2'2'cGAMP	2.8%	1.8	0.2	0.6
3'3'cGAMP	17%	1	0.3	1.4
3'3'c-diGMP	32%	0	0	0
2'3'cGAMP	1.1%	1	1	1

[a] Viability of monocytes in PBMC culture treated with 12.5µM CDN for 16 h. Viability of monocytes in untreated control equals 100%. Values are the mean of three independent determinations from one PBMC donor. [b] Levels of INF α, INF γ and TNFα secreted by PBMC treated with 12.5µM CDN for 16 h relative to levels secreted by PBMC treated with 12.5µM 2'3'cGAMP. Values are the mean of three independent determinations from the same PBMC donor as in monocyte cytotoxicity assay; Amount of cytokines induced by 2'3'cGAMP treatment: Interferon γ: 5570 pg/ml , TNFα: 5552 pg/ml, Interferon α: 648 pg/ml.

DISCUSSION AND CONCLUSIONS

In this study, we show that 2'3'CDNs can easily be prepared from NTP analogues by employing vertebrate cyclic dinucleotide synthase cGAS. We profiled substrate specificity of human, mouse and chicken cGAS and we developed a general protocol for enzymatic synthesis of CDNs. With few exceptions (*e.g.*, O^6-methyl-guanosine-triphosphate **(16)** which was an exclusive substrate of human cGAS), the mouse enzyme turned out to be the most promiscuous and was used for preparation of thirty-four CDNs. Principally, it should be possible to prepare more CDNs from our small library of NTPs. Majority of CDNs in this study contained either AMP as the 3' nucleotide or GMP as 2' nucleotide, and more CDNs where both nucleotides are analogues such as CDN-2, -4, -5 can be envisioned.

During our efforts to identify novel STING agonists,[38] we were guided rather by the digitonin than standard assay. As mentioned above, activity of CDNs is influenced by the efficiency of their uptake into cells in the latter assay. Consequently, EC_{50} values for the same CDN are at least 100-fold higher in the standard than digitonin assay (Table 2, 3, 4 and 6). The uptake issue can be ultimately solved by synthesis of lipophilic prodrugs of CDNs as presented in recent patent literature.[39]

An ideal CDN for clinical use should have similar activity toward all STING haplotypes; thus, eliminating the need for genotyping of patients. CDNs with adenine 3' nucleotide and guanine 2' nucleotide containing 2'-F or 3'-F substitutions or both (CDN-1, -2, and -3), 2'-F and 3'-deoxy groups (CDN-4) or 2'-deoxy and 3'-F substitutions (CDN-5) showed good activity across all STING haplotypes. In contrast to the general notion, not all 2'3'CDNs are good REF STING agonists.[33,34,40] CDNs with *ara*-adenosine, 2'-amino-2'-deoxyadenosine as 3' nucleotide and some of CDNs with 2'deoxyribonucleotides had diminished potency against REF STING. Substitutions

of nucleobases almost always resulted in impaired activation of REF STING haplotype with the only exception being CDN-29 where 2' nucleotide guanosine was replaced for inosine.

All prepared CDNs stimulated human PBMC to secret IFNα, IFNγ and TNFα, consistently with their ability to activate cGAS-STING pathway. In agreement with previously published data[37], CDNs decreased viability of monocytes in PBMC cultures without affecting T-lymphocytes (Table 7, S8). However, we cannot exclude that some other factors such as PBMC purification, cell density and/or cultivation conditions could exacerbate the negative effect of CDNs on monocytes. Monocytic cytotoxicity seemed to be somewhat proportional to the levels of induced cytokines (Table 7, S8). Unfortunately, no CDN inducing high levels of cytokines and low monocytic cytotoxicity was identified (Table 7, S8).

We used DSF measurements to rationalize interactions of CDN ligands with human WT STING. Crystal structures and docking calculations highlight large binding modes similarities of examined ligands. This suggests the effects of modifications on ΔT_m values will be dictated primarily by local environment. This notion is further supported by the additivity of $\Delta\Delta T_m$ values of ligands with multiple modifications. As a result, the inferred structure-activity relationships show good agreement with measured ΔT_m values in all cases.

Crucial element for understanding these relationships is the network of water molecules, which was obtained by combining information obtained from X-ray crystallography and computational modelling. Furthermore, estimates of differences in conformational strain of various ligands highlight that changes to the ligand affect not only its interactions with the protein but the ease of adapting the necessary conformation as well.

In summary, an enzymatic synthesis of 2'3'CDNs turned out to be an efficient way of generating SAR for CDNs and STING and can be employed beyond ribonucleotides as exemplified in recently published patent.[38]

EXPERIMENTAL SECTION

Materials

Adenosine-5'-O-(1-thiotriphosphate), 2-aminoadenosine-5'-triphosphate, 2-amino-6-chloropurine-5'-triphosphate, 2'-amino-2'-deoxy-adenosine-5'-triphosphate, 2-aminopurine-riboside-5'-triphosphate, ara-adenosine-5'-triphosphate, 8-azaadenosine-5‘-triphosphate, 8-azidoadenosine-5'-triphosphate, 7-deazaadenosine-5'-triphosphate, 7-deazaguanosine-5'-triphosphate, 2'-deoxyadenosine-5'-triphosphate, 2'-fluoro-2'-deoxyadenosine-5'-triphosphate, guanosine-5'-O-(1-thiotriphosphate), isoguanosine-5'-triphosphate, N6-methyladenosine-5'-triphosphate, 3'-O-methyladenosine-5'-triphosphate, N1-methyl-adenosine-5'-triphosphate, O6-methylguanosine-5'-triphosphate, 8-oxoadenosine-5'-triphosphate, 8-oxoguanosine-5'-triphosphate, thienoguanosine-5'-triphosphate, and xanthosine-5'-triphosphate were purchased from TriLink Biotechnologies (San Diego, USA). AICAR triphosphate, 2'-bromo-2'-deoxyadenosine-5'-triphosphate, 2'-chloro-2'-deoxyadenosine-5'-triphosphate, 3'-deoxyguanosine-5'-triphosphate, 2-fluoro-ara-adenosine-5'-triphosphate, 2'-iodo-2'-deoxyadenosine-5'-triphosphate, 6-mercaptopurineriboside-5'-triphosphate, 6-methylthioguanosine-5'-triphosphate, 6-methylthioinosine-5‘-triphosphate and 6-thioguanosine-5'-triphosphate were from Jena Bioscience (Jena, Germany). 2-fluoro-ara-adenosine-5'-triphosphate, 2'-deoxy-2-chloroadenosine-5’-triphosphate, 2'-deoxy-2,2'-difluoroadenosine 5’-triphosphate and 2'-deoxy-2-fluoroadenosine 5’-triphosphate were obtained from Metkinen Chemistry (Kuopio, Finland). Inosine-5‘-triphosphate and 7-methylguanosine-5'-triphosphate were from Sigma-Aldrich (Prague, Czech Republic). The other NTPs were prepared from commercially available nucleosides following a standard protocol.[41] SeQuant ZIC-pHILIC column was from Merck Millipore (Prague, Czech Republic). Luna column (5 μm C18 250x10 mm) was purchased from Phenomenex (Torrance, USA). Zombie NIR™ Fixable Viability Kit and BD Cytofix™ Fixation Buffer were supplied by

BioLegend (San Diego, USA). ProcartaPlex Assays and SYPRO Orange originated from Thermo Fisher Scientific(Waltham, USA).

Generation of 293T reporter cell lines stably expressing WT, HAQ, REF, AQ and Q STING haplotypes, purification of human, chicken, and mouse cGAS protein and human WT STING protein are detailed in Supporting Information.

Enzymatic Synthesis of CDNs

Nucleoside triphosphates (final concentration 1 mM) were incubated in 20 mM Tris-HCl buffer pH 8.0 containing 20 mM $MgCl_2$, 5 μM mouse, chicken or human cGAS, and 0.1 mg/ml herring testes DNA at 37 °C overnight in a shaker. The reaction mixtures were then spun at 25,000 g for 20 min and supernatants were passed through Pierce™ Protein Concentrators PES, 3K MWCO, 0.5 mL (Thermo Fisher Scientific, Prague, Czech Republic). In small scale reactions, the samples were directly analyzed by methods mentioned below. Reaction conversions were determined by HPLC using UV detection at 260 nm. Conversions are defined as follows; a ratio of AUC of a CDN over the sum of AUCs of the CDN, NTPs and NDPs.

In the case of large scale CDN synthesis, triethyl ammonium bicarbonate buffer (pH 8.5) was added to the flow-through fractions to 0.1 M final concentration, and CDNs were purified on semipreparative C18 column (Luna 5 μm C18 250x10 mm) using 50 min gradient at flow rate 3 mL/min of 0-10% acetonitrile in 0.1 M TEAB buffer (pH 8.5). TEAB was removed from the collected fractions by 3 cycles of evaporation/dissolving in 50% methanol and triethylammonium ion was exchanged for Na+ ion by slowly passing aqueous solution of the TEA+ salt through a DOWEX 50 (Na+ cycle) column and freeze-drying appropriate eluted fractions. The identification of CDNs was performed on ACQUITY UPLC® H-Class PLUS chromatographic system with MS SQ Detector 2 (Waters, Milford, USA) using iHILIC®-Fusion column SS 50 x 2.1mm, 1.8 μm

(HILICON AB, Sweden) and 20 mM ammonium acetate buffer pH 6.8 with linear gradient of acetonitrile (85 to 50 % in 4 min; flow rate 0.32 mL/min). Positive ESI method was used for ionization. Alternatively, CDNs were identified on Waters UPLC H-Class Core chromatographic system with MS QDa Detector (Waters, Milford, USA) using Acquity UPLC BEH C18 column 50 x 2.1 mm, 1.7 µm (Waters, Milford, USA) and 0.1% formic acid in water with linear gradient of acetonitrile (0 to 100 % in 7 min, flow rate 0.5 ml/min). Negative ESI method was used for ionization. Identification of CDNs was also performed on Waters UPLC chromatographic system with Q-TOF MS detector (Waters, Milford, USA) using SeQuant® ZIC®-pHILIC column 5 mm, polymeric, 50 x 2.1 mm (Merck, Darmstadt, Germany) and 10 mM ammonium acetate buffer pH 6.8 with linear gradient of acetonitrile (10 to 60 % in 7 min, flow rate 0.3 ml/min). Negative ESI method was used for ionization. Purity of all final compounds was >95% as determined by methods mentioned above. Large scale synthesis conversion rates of NTPs to CDNs and the enzymes used for reaction can be found in SI in Table S5.

NMR spectroscopy and High Resolution Mass Spectrometry Analysis

Proton NMR spectra (1D, 2D-H,H-COSY and 2D-H,H-ROESY) were measured on a Bruker 600 AVANCE III HD instrument (^{1}H at 600 MHz) equipped with 5 mm cryo-probe in D_2O at 25°C. Chemical shifts were referenced to dioxane (added as internal standard) and recalculated to δ-scale using δ_H(dioxane) = 3.75 ppm. The ^{31}P and ^{19}F NMR spectra were measured in D_2O at 25°C on a Bruker 500 AVANCE III HD instrument (^{31}P at 202.4 MHz and ^{19}F at 470.4 MHz frequency) in 5 mm cryo-probe and referenced to H_3PO_4 (^{31}P) and $CFCl_3$ (^{19}F) as external standards.

High Resolution Mass Spectrometry Analysis of prepared CDNs was performed on LTQ Orbitrap XL™ ETD Hybrid Ion Trap-Orbitrap Mass Spectrometer (Thermo Fisher Scientific). Negative ESI method was used for ionization.

Digitonin Assay with 293T reporter cells

293T reporter cells stably expressing different STING protein haplotypes (WT, HAQ, REF, AQ or Q) were seeded at density of 250,000 cells per cm^2 onto a 96 well white poly-D-lysine coated plates in 100 µl DMEM with high glucose supplemented with 10% heat inactivated FBS. The medium was removed the next day and three-fold serial dilutions of compounds in digitonin buffer containing 50 mM HEPES pH 7.0, 100 mM KCl, 3 mM $MgCl_2$, 0.1 mM DTT, 85 mM sucrose, 0.2% (w/w) BSA, 1 mM ATP, 0.1 mM GTP, and 10 µg/mL digitonin A were added to the cells. After 30 min incubation at 37°C with 5% CO_2, the digitonin buffer was removed, cells were washed once with 100 µl of cultivation medium, and 100 µl of fresh medium was added to each well. The plates with cells were further incubated for 5 h at 37°C with 5% CO_2. Thereafter 50 µl of the medium was removed and 30 µl of Bright-Glo™ Luciferase Assay System reagent was added to each well. Luminescence was measured on Spark® (TECAN, Grödig, Austria) and GraphPad Prism (La Jolla, USA) was used to calculate the 50% effective concentration (EC_{50}) from an 8-point dose-response curve. Representative dose response curves are shown in Figure S2. Nonlinear regression curve fit with standard slope was used for EC_{50} values calculations. The EC_{50} value represents CDN concentration that gives half-maximal response of firefly luciferase in 293T reporter assay. Maximum fold of firefly luciferase induction in 293T reporter assay did not differ among tested CDNs by more than 30 % compared to the natural STING ligand 2'3'cGAMP.

Standard Assay using 293T reporter cells

293T reporter cells stably expressing WT STING protein haplotype were seeded at density of 250,000 cells per cm^2 onto 96 well white poly-D-lysine coated plates in 100 µl DMEM with high glucose supplemented with 10% heat inactivated FBS. The next day medium was removed and 30 µl of serially diluted compounds in the cultivation medium were added to wells. After 7 h of incubation at 37°C with 5% CO_2, 20 µl of incubation medium and 30 µl of Bright-Glo™ Luciferase Assay System reagent were added to wells. Luminescence measurement and EC_{50} calculations were performed as described above.

Differential Scanning Fluorimetry with WT STING

WT STING protein was diluted to the final concentration 0.1 mg/ml in 100 mM Tris-HCl buffer pH 7.4 containing 150 mM NaCl, 1:500 (v/v) SYPRO Orange, 150 µM CDN or water. 20 µL solutions of the reaction mixtures were pipetted in triplicates into 96 well optical plates and thermal denaturation of samples was performed on real time PCR cycler (LightCycler ® 480 Instrument II – Roche, Basel, Switzerland). The first derivative of the thermal denaturation curves was performed to calculate melting temperatures (T_m's) of STING – CDN complexes and STING protein alone. The thermal shift (ΔT_m) for each CDN was calculated by subtracting the average denaturing temperature of STING without CDN from the average denaturing temperature of STING-CDN complex.

Peripheral Blood Mononuclear Cell Assay

Buffy coats from healthy individuals were obtained from the Institute of Hematology and Blood Transfusion (Prague, Czech Republic). Informed written consent was obtained from each individual enrolled. PBMC were isolated from fresh buffy coats using Ficoll density gradient

centrifugation (Ficoll® Paque Plus, GE Healthcare) in SepMate tubes (SepMateTM PBMC Isolation Tubes, Stemcell Technologies). Freshly isolated PBMC were washed with PBS containing 2mM EDTA, and 500,000 cells were seeded into a well in RPMI 1640 medium supplemented with 10% (v/v) fetal bovine serum into U-shaped 96 well plates ($5x10^6$ cells/mL). CDNs were added to the final concentration of 12.5 μM, and after a 16 h-incubation time at 37 °C in 5% CO_2 atmosphere, culture medium was collected for cytokine analyses. The levels of secreted INFα, INFγ and TNFα were determined with ProcartaPlex Assays using MAGPIX System (Merck KGaA, Darmstadt, Germany) according to manufacturer's instruction. Culture medium served as a negative control and values are represented as a fold of 2'3'cGAMP induced cytokine values. Cells were then harvested and flow cytometry was performed for phenotype determination. PBMC were pre-stained with live/dead marker Zombie-NIR at 1:100 dilution for 20 min at room temperature. Specific staining was carried out with following mouse anti-human monoclonal antibodies: CD3-APC (1:100 dilution, OKT3 clone, Tonbo Biosciences), CD14-PE (1:50 dilution, clone 61D3, Tonbo Biosciences). Cells were incubated with the antibody mixture or appropriate isotype controls for 30 min at 4°C in PBS supplemented with 0.5% BSA. Then they were fixed with BD Cytofix™ Fixation Buffer and kept at 4 °C until assayed. Data were acquired on a BD LSR Fortessa cytometer (BD Biosciences) using FACS Diva software (version 7, BD Biosciences). Debris were excluded by forward/side scatter gating followed by doublet and dead cell exclusion. Population of interest was gated on specific CD3 negative CD14 positive monocytes or CD3 positive T-lymphocytes in live population. Data were analyzed using FlowJo™ software (version 10, FlowJo LLc, Ashland, OR, USA).

Crystallization and crystallographic analysis

Sitting drop vapor diffusion protocol was used for setting up drops of the mixture of 1mM WT STING and 0.5 mM CDN-1 or CDN-24 supplemented with 10mM EDTA. The crystals grew in drops consisting of 1:1 mixture of protein:ligand complexes and well solution consisting of 0.2 M $CaCl_2$, and 20% (w/v) PEG 3350 in the case of CDN-1 or 1.6 M NaH_2PO_4/0.4 M K_2HPO_4, and 0.1 M phosphate-citrate buffer pH 4.2 for CDN-24. Crystals were cryo-protected in the mother liquor supplemented with 20% (v/v) glycerol and flash frozen in liquid nitrogen. A single frozen crystal was used for X-ray dataset collection using the home-source or BESSY ID 14-2.[42] Processing of the datasets (integration and scaling) was done by XDS.[43] The structures were solved using the program Phaser[44] of the CCP4 package and molecular replacement strategy (MR) with structure of STING (pdb code: 4KSY) as a search model. Ligands were placed in their electron densities by Coot.[45] The structures were refined using Phenix (XYZ coordinates and Real-space refinement)[46] and figures were generated using PyMol software.[47] The structures were deposited in the Protein Data Bank, (www.pdb.org) under accession code 6S27 and 6S26.

Conformational Sampling

The ligands were sampled using PRIME algorithm[48] (employing "thorough" setting) as implemented in Schrodinger 2019-1 suite.[49] Obtained structures were subjected to optimization using the Becke-Perdew 86 (BP86) exchange-correlation functional[50–52] Ahlrichs' def-TZVP basis set,[53] the empirical dispersion correction with zero-damping[54] (denoted as D3) and conductor-like screening model (COSMO) for implicit solvation, with $\varepsilon_r = 80$ corresponding to dielectric constant of water. The single-point energies were calculated using the BP86-D3 and the def2-TZVPD basis set. Both structure optimizations and single-point energies were obtained with TurboMole 7.2 program suite.[55] Solvation (free) energies were calculated using COSMO-RS method[56,57]

(conductor-like screening model for realistic solvation) as implemented in COSMOthermX17,[58] employing "BP_TZVPD_FINE_C30_1701.ctd" parametrization file, FINE cavities ($cosmo_isorad keyword) with $\varepsilon_r = \infty$ (ideal conductor). The conformational (strain) energy was obtained as difference between the total energy (i.e. sum of single-point and solvation energies) of the bound structure (obtained from QM/MM) and the lowest total free energy of all conformers obtained from conformational sampling.

QM/MM Methods

Protein Setup. For QM/MM modeling, we employed the X-ray structure of the STING protein complexes with cyclic [FdA(3',5')pFdA(3',5')p] deposited in the Protein Data Bank, (www.pdb.org) under accession code 6T1X, applying appropriate symmetry operation from raw X-ray data. An initial model was built within the YASARA modelling package.[59] H atoms were added to the protein to mimic neutral pH and their positions were optimized. The glycerol and water molecules were removed from the model. The parameter set used for the protein was AMBER ff03.[60] The ligand was optimized in a vacuum and partial charges on its atoms were obtained by a restrained fit to the electrostatic potential (RESP) at the AM1BCC level.[61]

The YASARA refined model was further equilibrated within the water solvation shell of $R = 41$ Å and subjected to simulated annealing and minimization according to standard protocols mentioned in the detail in the Supporting Information. The quantum system consisted of approximately 600 atoms (~70 atoms of the ligands, 18 water molecules, and 486 atoms of the STING protein which included all interacting residues in the vicinity of the ligand; the 3-D structures of the QM systems in QM/MM calculations for studied ligands are deposited in the Supplementary material in the PDB format).

In the QM/MM calculations, the standard hydrogen-link atom approach was used, the quantum system was treated at the BP86-D3/DZVP-DFT level, while the MM system was described by the same force field as used in the YASARA (Amber ff03). The QM/MM calculations were done employing ComQum software.[62] Further details are mentioned in the Supplementary material.

Ancillary Information.

ASSOCIATED CONTENT

Supporting Information

1. Supplemental materials
2. Supplemental methods
   - Cloning of pUNO1- hSTING-AQ, -Q, and -REF plasmids.
   - Cloning of pGL64.27-4xISRE plasmid.
   - Development of 293T reporter cells.
   - Cloning and expression of WT STING protein.
   - Cloning of cGAS enzymes.
   - Expression and Purification of cGAS enzymes.
   - Synthesis of CDN-29.
   - Synthesis of CDN-35, -36, -37.
   - Molecular docking.
   - Details of QM/MM Calculations.
3. Supplemental data

Table S1a. The ^{1}H, ^{31}P and ^{19}F NMR data of 2‘,3‘-CDNs **1 – 3** and **7 – 11** in D_2O.
Table S1b. The ^{1}H, ^{31}P and ^{19}F NMR data of 2‘,3‘-deoxy CDNs **4 – 6** and **12 – 15** in D_2O.
Table S2. The ^{1}H and ^{31}P NMR data of 2‘,3‘-CDNs **16 - 26** in D_2O.
Table S3. The ^{1}H and ^{31}P NMR data of 2‘,3‘-CDNs **27 - 32** in D_2O.
Table S4. The ^{1}H and ^{31}P NMR data of 2‘,3‘-CDNs with thiophosphate groups **33 - 37** in D_2O.
Table S5. Yields of CDNs from enzymatic preparation and their HRMS data for prepared CDNs analysis.
Table S6. Crystallography data collection and processing.
Table S7. Crystallography structure solution and refinement.
Table S8. Effect of CDNs on CD14+ monocyte and CD3+ T-cell populations and cytokine induction in PBMC Assay (Donor 2).
Figure S1. Correlation of ΔTm values from DSF Assay and EC_{50} values from Standard or Digitonin Assay of prepared CDNs.
Figure S2. Representative dose response curves of 5 CDNs from Digitonin Assay on WT or REF STING haplotypes.
Supplementary files
- Molecular Formula Strings
- Structures obtained from computational modelling

Accession Codes

PDB code for human STING with bound CDN-1 and CDN-24 are 6S27 and 6S26, respectively.

Corresponding Author Information:

Gabriel.Birkus@uochb.cas.cz Phone: (+420) 770-125-014.

Acknowledgements

The work was supported by Gilead Sciences, Inc., from European Regional Development Fund; OP RDE; Project: "Chemical biology for drugging undruggable targets" (ChemBioDrug, No. CZ.02.1.01/0.0/0.0/16_019/0000729), and the Grant Agency of the Czech Republic (grant 20-08772S). Computational resources were provided by the IT4Innovations National Supercomputing Center (project LM2015070) and CESNET MetaCentrum (project LM2015042). Our special thanks belong to MSc Kvetoslava Kertisová for her kind assistance with HRMS spectra and Mrs. Hana Prouzová for help with biochemical assays. We also thank Kamil Hercík, PhD for providing us with plasmid construct used for production of STING protein for crystallographic analysis. We also would like to thank HZB for the allocation of synchrotron radiation beamtime.

Abbreviations Used

2D-H,H-COSY, two-dimensional homonulear correlation spectroscopy; 2D-H,H-ROESY, two-dimensional homonulear rotating Overhauser effect spectroscopy; AMP, adenosine-monophosphate; AUC, Area under curve; BSA, bovine serum albumin; CDN, cyclic dinucleotide; DCA, dichloroacetic acid; DCM, dichloromethane; dsDNA, double stranded DNA; DSF, differential scanning fluorimetry; FBS, fetal bovine serum; cGAS, cyclic guanosine adenosine synthase; GMP, guanosine-monophosphate; IFN, interferon; IL-6, Interleukin 6; IRF3, Interferon regulatory factor 3; PBMC, peripheral blood mononuclear cells; PBS, phosphate-buffered saline; STING, stimulator of interferon genes; MP, monophosphate; MS, mass spectroscopy; NDP,

nucleotide-5'-diphosphate; NFκB, nuclear factor kappa-light-chain-enhancer of activated B cells; NOE, nuclear Overhauser effect; NTP, nucleotide-5'-triphosphate; PEG, polyethylene glycol; TBK1, TANK binding kinase; TEAB, triethylammonium bicarbonate; TNFα, tumor necrosis factor α.

REFERENCES

(1) Danilchanka, O.; Mekalanos, J. J. Cyclic Dinucleotides and the Innate Immune Response. *Cell* **2013**, *154* (5), 962–970. https://doi.org/10.1016/j.cell.2013.08.014.

(2) Sun, L.; Wu, J.; Du, F.; Chen, X.; Chen, Z. J. Cyclic GMP-AMP Synthase Is a Cytosolic DNA Sensor That Activates the Type-I Interferon Pathway. *Science* **2013**, *339* (6121), 786–791. https://doi.org/10.1126/science.1232458.

(3) Römling, U.; Galperin, M. Y.; Gomelsky, M. Cyclic Di-GMP: The First 25 Years of a Universal Bacterial Second Messenger. *Microbiol. Mol. Biol. Rev. MMBR* **2013**, *77* (1), 1–52. https://doi.org/10.1128/MMBR.00043-12.

(4) Corrigan, R. M.; Abbott, J. C.; Burhenne, H.; Kaever, V.; Gründling, A. C-Di-AMP Is a New Second Messenger in Staphylococcus Aureus with a Role in Controlling Cell Size and Envelope Stress. *PLoS Pathog.* **2011**, *7* (9), e1002217. https://doi.org/10.1371/journal.ppat.1002217.

(5) Davies, B. W.; Bogard, R. W.; Young, T. S.; Mekalanos, J. J. Coordinated Regulation of Accessory Genetic Elements Produces Cyclic Di-Nucleotides for V. Cholerae Virulence. *Cell* **2012**, *149* (2), 358–370. https://doi.org/10.1016/j.cell.2012.01.053.

(6) Ross, P.; Weinhouse, H.; Aloni, Y.; Michaeli, D.; Weinberger-Ohana, P.; Mayer, R.; Braun, S.; de Vroom, E.; van der Marel, G. A.; van Boom, J. H., Benziman, M. Regulation of Cellulose Synthesis in Acetobacter Xylinum by Cyclic Diguanylic Acid. *Nature* **1987**, *325 (6101)*, 279–281.

(7) Ablasser, A.; Goldeck, M.; Cavlar, T.; Deimling, T.; Witte, G.; Röhl, I.; Hopfner, K.-P.; Ludwig, J.; Hornung, V. cGAS Produces a 2'-5'-Linked Cyclic Dinucleotide Second Messenger That Activates STING. *Nature* **2013**, *498* (7454), 380–384. https://doi.org/10.1038/nature12306.

(8) Zhang, X.; Shi, H.; Wu, J.; Zhang, X.; Sun, L.; Chen, C.; Chen, Z. J. Cyclic GMP-AMP Containing Mixed Phosphodiester Linkages Is an Endogenous High-Affinity Ligand for STING. *Mol. Cell* **2013**, *51* (2), 226–235. https://doi.org/10.1016/j.molcel.2013.05.022.

(9) Wu, X.; Wu, F.-H.; Wang, X.; Wang, L.; Siedow, J. N.; Zhang, W.; Pei, Z.-M. Molecular Evolutionary and Structural Analysis of the Cytosolic DNA Sensor cGAS and STING. *Nucleic Acids Res.* **2014**, *42* (13), 8243–8257. https://doi.org/10.1093/nar/gku569.

(10) Gallucci, S.; Maffei, M. E. DNA Sensing across the Tree of Life. *Trends Immunol.* **2017**, *38* (10), 719–732. https://doi.org/10.1016/j.it.2017.07.012.

(11) Gao, P.; Ascano, M.; Wu, Y.; Barchet, W.; Gaffney, B. L.; Zillinger, T.; Serganov, A. A.; Liu, Y.; Jones, R. A.; Hartmann, G.; Tuschl, T.; Patel, D. J. Cyclic [G(2',5')PA(3',5')p] Is the Metazoan Second Messenger Produced by DNA-Activated Cyclic GMP-AMP Synthase. *Cell* **2013**, *153 (5)*, 1094–1107. https://doi.org/10.1016/j.cell.2013.04.046.

(12) Ishikawa, H.; Barber, G. N. STING Is an Endoplasmic Reticulum Adaptor That Facilitates Innate Immune Signalling. *Nature* **2008**, *455* (7213), 674–678. https://doi.org/10.1038/nature07317.

(13) Tsuchiya, Y.; Jounai, N.; Takeshita, F.; Ishii, K. J.; Mizuguchi, K. Ligand-Induced Ordering of the C-Terminal Tail Primes STING for Phosphorylation by TBK1. *EBioMedicine* **2016**, *9*, 87–96. https://doi.org/10.1016/j.ebiom.2016.05.039.

(14) Liu, S.; Cai, X.; Wu, J.; Cong, Q.; Chen, X.; Li, T.; Du, F.; Ren, J.; Wu, Y.-T.; Grishin, N. V.; Zhijan, J. Ch. Phosphorylation of Innate Immune Adaptor Proteins MAVS, STING, and TRIF Induces IRF3 Activation. *Science* **2015**, *347 (6227)*, aaa2630. https://doi.org/10.1126/science.aaa2630.

(15) Shang, G.; Zhang, C.; Chen, Z. J.; Bai, X.-C.; Zhang, X. Cryo-EM Structures of STING Reveal Its Mechanism of Activation by Cyclic GMP-AMP. *Nature* **2019**, *567* (7748), 389–393. https://doi.org/10.1038/s41586-019-0998-5.

(16) Zhang, C.; Shang, G.; Gui, X.; Zhang, X.; Bai, X.-C.; Chen, Z. J. Structural Basis of STING Binding with and Phosphorylation by TBK1. *Nature* **2019**, *567* (7748), 394–398. https://doi.org/10.1038/s41586-019-1000-2.

(17) Zhao, B.; Du, F.; Xu, P.; Shu, C.; Sankaran, B.; Bell, S. L.; Liu, M.; Lei, Y.; Gao, X.; Fu, X.; Zhu, F.; Liu, Y.; Laganowsky, A.; Zheng, X.; Ji, J.-Y.; West, A. P.; Watson, R. O.; Li, P. A Conserved

PLPLRT/SD Motif of STING Mediates the Recruitment and Activation of TBK1. *Nature* **2019**, *569 (7758)*, 718–722. https://doi.org/10.1038/s41586-019-1228-x.

(18) Fang, R.; Wang, C.; Jiang, Q.; Lv, M.; Gao, P.; Yu, X.; Mu, P.; Zhang, R.; Bi, S.; Feng, J.-M.; et al. NEMO-IKKβ Are Essential for IRF3 and NF-KB Activation in the cGAS-STING Pathway. *J. Immunol. Baltim. Md 1950* **2017**, *199* (9), 3222–3233. https://doi.org/10.4049/jimmunol.1700699.

(19) Musella, M.; Manic, G.; De Maria, R.; Vitale, I.; Sistigu, A. Type-I-Interferons in Infection and Cancer: Unanticipated Dynamics with Therapeutic Implications. *Oncoimmunology* **2017**, *6* (5), e1314424. https://doi.org/10.1080/2162402X.2017.1314424.

(20) Study of MK-1454 Alone or in Combination With Pembrolizumab in Participants With Advanced/Metastatic Solid Tumors or Lymphomas (MK-1454-001) - Full Text View - ClinicalTrials.gov https://clinicaltrials.gov/ct2/show/NCT03010176 (accessed Jun 19, 2019).

(21) Safety and Efficacy of MIW815 (ADU-S100) +/- Ipilimumab in Patients With Advanced/Metastatic Solid Tumors or Lymphomas - Full Text View - ClinicalTrials.gov https://clinicaltrials.gov/ct2/show/NCT02675439 (accessed Jun 19, 2019).

(22) Li, X.-D.; Wu, J.; Gao, D.; Wang, H.; Sun, L.; Chen, Z. J. Pivotal Roles of cGAS-CGAMP Signaling in Antiviral Defense and Immune Adjuvant Effects. *Science* **2013**, *341* (6152), 1390–1394. https://doi.org/10.1126/science.1244040.

(23) Barber, G. N. STING: Infection, Inflammation and Cancer. *Nat. Rev. Immunol.* **2015**, *15* (12), 760–770. https://doi.org/10.1038/nri3921.

(24) Gaffney, B. L.; Veliath, E.; Zhao, J.; Jones, R. A. One-Flask Syntheses of c-Di-GMP and the [Rp,Rp] and [Rp,Sp] Thiophosphate Analogues. *Org. Lett.* **2010**, *12* (14), 3269–3271. https://doi.org/10.1021/ol101236b.

(25) Clivio, P.; Coantic-Castex, S.; Guillaume, D. (3'-5')-Cyclic Dinucleotides: Synthetic Strategies and Biological Potential. *Chem. Rev.* **2013**, *113* (10), 7354–7401. https://doi.org/10.1021/cr300011s.

(26) Gillis, E. P.; Eastman, K. J.; Hill, M. D.; Donnelly, D. J.; Meanwell, N. A. Applications of Fluorine in Medicinal Chemistry. *J. Med. Chem.* **2015**, *58* (21), 8315–8359. https://doi.org/10.1021/acs.jmedchem.5b00258.

(27) Launer-Felty, K. D.; Strobel, S. A. Enzymatic Synthesis of Cyclic Dinucleotide Analogs by a Promiscuous Cyclic-AMP-GMP Synthetase and Analysis of Cyclic Dinucleotide Responsive Riboswitches. *Nucleic Acids Res.* **2018**, *46* (6), 2765–2776. https://doi.org/10.1093/nar/gky137.

(28) Li, F.; Cimdins, A.; Rohde, M.; Jänsch, L.; Kaever, V.; Nimtz, M.; Römling, U. DncV Synthesizes Cyclic GMP-AMP and Regulates Biofilm Formation and Motility in Escherichia Coli ECOR31. *mBio* **2019**, *10* (2), e02492-02418. https://doi.org/10.1128/mBio.02492-18.

(29) Kranzusch, P. J.; Lee, A. S. Y.; Wilson, S. C.; Solovykh, M. S.; Vance, R. E.; Berger, J. M.; Doudna, J. A. Structure-Guided Reprogramming of Human cGAS Dinucleotide Linkage Specificity. *Cell* **2014**, *158* (5), 1011–1021. https://doi.org/10.1016/j.cell.2014.07.028.

(30) Li, L.; Yin, Q.; Kuss, P.; Maliga, Z.; Millán, J. L.; Wu, H.; Mitchison, T. J. Hydrolysis of 2'3'-CGAMP by ENPP1 and Design of Nonhydrolyzable Analogs. *Nat. Chem. Biol.* **2014**, *10* (12), 1043–1048. https://doi.org/10.1038/nchembio.1661.

(31) Altschul, S. F.; Gish, W.; Miller, W.; Myers, E. W.; Lipman, D. J. Basic Local Alignment Search Tool. *J. Mol. Biol.* **1990**, *215* (3), 403–410. https://doi.org/10.1016/S0022-2836(05)80360-2.

(32) Khiar, S.; Lucas-Hourani, M.; Nisole, S.; Smith, N.; Helynck, O.; Bourgine, M.; Ruffié, C.; Herbeuval, J.-P.; Munier-Lehmann, H.; Tangy, F.; Vidalain, Pierre-Olivier. Identification of a Small Molecule That Primes the Type I Interferon Response to Cytosolic DNA. *Sci. Rep.* **2017**, 7, 2561. https://doi.org/10.1038/s41598-017-02776-z.

(33) Yi, G.; Brendel, V. P.; Shu, C.; Li, P.; Palanathan, S.; Cheng Kao, C. Single Nucleotide Polymorphisms of Human STING Can Affect Innate Immune Response to Cyclic Dinucleotides. *PloS One* **2013**, *8* (10), e77846. https://doi.org/10.1371/journal.pone.0077846.

(34) Patel, S.; Jin, L. TMEM173 Variants and Potential Importance to Human Biology and Disease. *Genes Immun.* **2019**, *20* (1), 82–89. https://doi.org/10.1038/s41435-018-0029-9.

(35) Dassault Systèmes BIOVIA. *Discovery Studio*; 2017 R2; Dassault Systèmes: San Diego, 2017.

(36) Smola, M.; Birkus, G.; Boura, E. No Magnesium Is Needed for Binding of the Stimulator of Interferon Genes to Cyclic Dinucleotides. *Acta Crystallogr. Sect. F Struct. Biol. Commun.* **2019**, *75* (Pt 9), 593–598. https://doi.org/10.1107/S2053230X19010999.

(37) Tosolini, M.; Pont, F.; Bétous, D.; Ravet, E.; Ligat, L.; Lopez, F.; Poupot, M.; Poirot, M.; Pérouzel, É.; Tiraby, G.; Verhoeyen, E.; Fournié, J.-J. Human Monocyte Recognition of Adenosine-Based Cyclic Dinucleotides Unveils the A2a Gαs Protein-Coupled Receptor Tonic Inhibition of Mitochondrially Induced Cell Death. *Mol. Cell. Biol*. **2015**, *35 (2)*, 479–495. https://doi.org/10.1128/MCB.01204-14.

(38) Birkuš, G.; Páv, O.; Jandušík, T.; Rosenberg, I.; Nencka, R. 2'3' Cyclic Dinucleotides with Phosphonate Bond Activating the STING Adaptor Protein. US20190185510, June 20, 2019.

(39) Iyer, R. P.; Sheri, A.; Padmanabhan, S.; Meher, G.; Zhou, S.; Challa, S.; Gimi, R. H.; Cleary, D. Compounds, Compositions, and Methods for the Treatment of Disease. WO2018009652A1, August 29, 2019.

(40) Diner, E. J.; Burdette, D. L.; Wilson, S. C.; Monroe, K. M.; Kellenberger, C. A.; Hyodo, M.; Hayakawa, Y.; Hammond, M. C.; Vance, R. E. The Innate Immune DNA Sensor cGAS Produces a Noncanonical Cyclic Dinucleotide That Activates Human STING. *Cell Rep.* **2013**, *3* (5), 1355–1361. https://doi.org/10.1016/j.celrep.2013.05.009.

(41) Gillerman, I.; Fischer, B. An Improved One-Pot Synthesis of Nucleoside 5'-Triphosphate Analogues. *Nucleosides Nucleotides Nucleic Acids* **2010**, *29* (3), 245–256. https://doi.org/10.1080/15257771003709569.

(42) Mueller, U.; Darowski, N.; Fuchs, M. R.; Förster, R.; Hellmig, M.; Paithankar, K. S.; Pühringer, S.; Steffien, M.; Zocher, G.; Weiss, M. S. Facilities for Macromolecular Crystallography at the Helmholtz-Zentrum Berlin. *J. Synchrotron Radiat.* **2012**, *19* (Pt 3), 442–449. https://doi.org/10.1107/S0909049512006395.

(43) Kabsch, W. XDS. *Acta Crystallogr. D Biol. Crystallogr.* **2010**, *66* (Pt 2), 125–132. https://doi.org/10.1107/S0907444909047337.

(44) McCoy, A. J.; Grosse-Kunstleve, R. W.; Adams, P. D.; Winn, M. D.; Storoni, L. C.; Read, R. J. Phaser Crystallographic Software. *J. Appl. Crystallogr.* **2007**, *40* (Pt 4), 658–674. https://doi.org/10.1107/S0021889807021206.

(45) Debreczeni, J. É.; Emsley, P. Handling Ligands with Coot. *Acta Crystallogr. D Biol. Crystallogr.* **2012**, *68* (Pt 4), 425–430. https://doi.org/10.1107/S0907444912000200.

(46) Adams, P. D.; Afonine, P. V.; Bunkóczi, G.; Chen, V. B.; Davis, I. W.; Echols, N.; Headd, J. J.; Hung, L.-W.; Kapral, G. J.; Grosse-Kunstleve, R. W.; McCoy, A. J.; Moriarty, N. W.; Oeffner, R.; Read, R.J.; Richardson, D. C.; Richardson, J. S.; Terwilinger, T. C.; Zwart, P. H. PHENIX: A Comprehensive Python-Based System for Macromolecular Structure Solution. *Acta Crystallogr. D Biol. Crystallogr.* **2010**, *66 (Pt 2)*, 213–221. https://doi.org/10.1107/S0907444909052925.

(47) Schrödinger LLC. *PyMOL*; The PyMOL Molecular Graphics System, Version 1.3r1; 2010.

(48) Sindhikara, D.; Spronk, S. A.; Day, T.; Borrelli, K.; Cheney, D. L.; Posy, S. L. Improving Accuracy, Diversity, and Speed with Prime Macrocycle Conformational Sampling. *J. Chem. Inf. Model.* **2017**, *57* (8), 1881–1894. https://doi.org/10.1021/acs.jcim.7b00052.

(49) Schrödinger LLC. *Maestro*; Schrödinger Release 2019-2; Schrödinger Suites: New York, NY, 2019.

(50) Becke, A. D. Density-Functional Exchange-Energy Approximation with Correct Asymptotic Behavior. *Phys. Rev. Gen. Phys.* **1988**, *38* (6), 3098–3100.

(51) Vosko, S. H.; Wilk, L.; Nusair, M. Accurate Spin-Dependent Electron Liquid Correlation Energies for Local Spin Density Calculations: A Critical Analysis. *Can. J. Phys.* **1980**, *58* (8), 1200–1211. https://doi.org/10.1139/p80-159.

(52) Perdew, J. P. Density-Functional Approximation for the Correlation Energy of the Inhomogeneous Electron Gas. *Phys. Rev. B Condens. Matter* **1986**, *33* (12), 8822–8824. https://doi.org/10.1103/physrevb.33.8822.

(53) Weigend, F.; Ahlrichs, R. Balanced Basis Sets of Split Valence, Triple Zeta Valence and Quadruple Zeta Valence Quality for H to Rn: Design and Assessment of Accuracy. *Phys. Chem. Chem. Phys. PCCP* **2005**, *7* (18), 3297–3305. https://doi.org/10.1039/b508541a.

(54) Grimme, S.; Antony, J.; Ehrlich, S.; Krieg, H. A Consistent and Accurate Ab Initio Parametrization of Density Functional Dispersion Correction (DFT-D) for the 94 Elements H-Pu. *J. Chem. Phys.* **2010**, *132* (15), 154104. https://doi.org/10.1063/1.3382344.

(55) *TURBOMOLE 7.2 2017, a Development of the University of Karlsruhe and Forschungszentrum Karlsruhe GmbH 1989−2007, TURBOMOLE GmbH since 2007*.

(56) Klamt, A. Conductor-like Screening Model for Real Solvents: A New Approach to the Quantitative Calculation of Solvation Phenomena. *J. Phys. Chem.* **1995**, *99* (7), 2224–2235. https://doi.org/10.1021/j100007a062.

(57) Klamt, A.; Jonas, V.; Bürger, T.; Lohrenz, J. C. W. Refinement and Parametrization of COSMO-RS. *J. Phys. Chem. A* **1998**, *102* (26), 5074–5085. https://doi.org/10.1021/jp980017s.

(58) Eckert, F.; Klamt, A. *COSMOthermX17*; Version C3.0, Release 15.01; COSMOlogic GmbH & Co. KG: Leverkusen, Germany, 2014.

(59) Krieger, E.; Joo, K.; Lee, J.; Lee, J.; Raman, S.; Thompson, J.; Tyka, M.; Baker, D.; Karplus, K. Improving Physical Realism, Stereochemistry, and Side-Chain Accuracy in Homology Modeling: Four Approaches That Performed Well in CASP8. *Proteins* **2009**, *77 Suppl 9*, 114–122. https://doi.org/10.1002/prot.22570.

(60) Duan, Y.; Wu, C.; Chowdhury, S.; Lee, M. C.; Xiong, G.; Zhang, W.; Yang, R.; Cieplak, P.; Luo, R.; Lee, T.; Caldwell, J.; Wang, J.; Kollman, P. A Point-Charge Force Field for Molecular Mechanics Simulations of Proteins Based on Condensed-Phase Quantum Mechanical Calculations. *J. Comput. Chem.* **2003**, *24 (16)*, 1999–2012. https://doi.org/10.1002/jcc.10349.

(61) Jakalian, A.; Jack, D. B.; Bayly, C. I. Fast, Efficient Generation of High-Quality Atomic Charges. AM1-BCC Model: II. Parameterization and Validation. *J. Comput. Chem.* **2002**, *23* (16), 1623–1641. https://doi.org/10.1002/jcc.10128.

(62) Ryde, U.; Olsson, M. H. M. Structure, Strain, and Reorganization Energy of Blue Copper Models in the Protein. *Int. J. Quantum Chem.* **2001**, *81* (5), 335–347. https://doi.org/10.1002/1097-461X(2001)81:5<335::AID-QUA1003>3.0.CO;2-Q.

Table of Contents graphic